Molecular Simulation

ISSN: (Print) (Online) Journal homepage: https://www.tandfonline.com/loi/gmos20

Temperature and its control in molecular dynamics simulations

M. Sri Harish & Puneet Kumar Patra

To cite this article: M. Sri Harish & Puneet Kumar Patra (2021) Temperature and its control in molecular dynamics simulations, Molecular Simulation, 47:9, 701-729, DOI: 10.1080/08927022.2021.1907382

To link to this article: https://doi.org/10.1080/08927022.2021.1907382

Published online: 31 Mar 2021.

Submit your article to this journal

Article views: 178

View related articles

View Crossmark data

Citing articles: 1 View citing articles

Full Terms & Conditions of access and use can be found at
https://www.tandfonline.com/action/journalInformation?journalCode=gmos20

MOLECULAR SIMULATION
2021, VOL. 47, NO. 9, 701–729
https://doi.org/10.1080/08927022.2021.1907382

Taylor & Francis
Taylor & Francis Group

Check for updates

Temperature and its control in molecular dynamics simulations

M. Sri Harish[a] and Puneet Kumar Patra [b]

[a]Department of Civil Engineering, Indian Institute of Technology Kharagpur, Kharagpur, West Bengal, India; [b]Department of Civil Engineering and Center for Theoretical Studies, Indian Institute of Technology Kharagpur, Kharagpur, West Bengal, India

ABSTRACT

The earliest molecular dynamics simulations relied on solving the Newtonian or equivalently the Hamiltonian equations of motion for a system. While pedagogically very important as the total energy is preserved in these simulations, they lack any relationship with real-life experiments, as most of these tests are performed in a constant temperature environment that allows energy exchanges. So, within the framework of molecular dynamics, the Newtonian evolution equations need to be modified to enable energy exchange between the system and the surroundings. The prime motive behind allowing energy exchange is to control the temperature of the system. Depending on the temperature being controlled and the modifications made to the equations of motion, different evolution equations, or thermostat algorithms, can be obtained. This work reviews the recent developments in controlling temperature through deterministic algorithms. We highlight the physical basis behind the algorithms, their advantages, and disadvantages, along with the situations where they are applicable. The review ends with a brief discussion on open-ended questions related to thermostatted dynamics.

ARTICLE HISTORY
Received 4 June 2020
Accepted 8 March 2021

KEYWORDS
Temperature; thermostats; molecular dynamics; ergodicity

1. Introduction

The computer revolution of the last century has fundamentally altered scientific research. With increasing computational power, researchers can build and test complex situations, which otherwise would have remained unexplored. The importance of computational modelling has been such that it has been adopted across disciplines as broad as physical sciences, chemical sciences, biological sciences, engineering, economics, etc., and now, techniques exist for solving problems at all known length scales – smooth particle hydrodynamics at astronomical scales, finite element method at macroscales, Monte-Carlo, and molecular dynamics at the atomic scale, density functional theory at the quantum scale, etc.

At atomistic scales, molecular dynamics (MD) has become one of the most popular techniques. MD simulations are powerful, only limited by the availability of computational resources. In MD, the temporal and spatial evolution of individual atoms and molecules (particles) are computed to obtain in-depth insights into the properties of a system and make several testable predictions about it. Consider an isolated system comprising N particles, with a Hamiltonian given by:

$$H = \sum_{i=1}^{3N} \frac{p_i^2}{2m} + \Phi(x_1, x_2, \ldots x_{3N}), \tag{1}$$

where, x_i and p_i denote the position and the momentum of the ith particle, and $\Phi(\ldots)$ denotes the potential energy of the system. For simplicity, all particles are assumed to have the same mass m. The equations of motion of such a system are given by [1]:

$$\frac{\mathrm{d}x_i}{\mathrm{d}t} = \frac{\partial H}{\partial p_i} = \frac{p_i}{m}, \quad \frac{\mathrm{d}p_i}{\mathrm{d}t} = -\frac{\partial H}{\partial x_i} = -\frac{\partial \Phi}{\partial x_i}. \tag{2}$$

Traditionally, in MD simulations these $6N$ equations are integrated in time to provide the system's trajectory. One of the simplest and most popular symplectic time integration algorithms is the Velocity-Verlet algorithm [2], which propagates the positions and momenta in time through:

$$\begin{aligned} x_i(t+\Delta t) &= x_i(t) + \frac{p_i(t)}{m}\Delta t + \frac{1}{2}\frac{F_i(t)}{m}\Delta t^2, \\ p_i(t+\Delta t) &= p_i(t) + \frac{1}{2}[F_i(t) + F_i(t+\Delta t)]\Delta t. \end{aligned} \tag{3}$$

Here $F_i = -\frac{\partial \Phi}{\partial x_i}$ is the force experienced by the ith particle. Since the system is isolated from the surroundings, these simulations preserve the total energy. The linear momentum is also conserved by these Newtonian equations. Thus, the trajectories obtained from these MD simulations are concomitant with a subset of the micro-canonical (NVE) ensemble encountered in statistical mechanics; the link between the two being provided by the ergodic hypothesis.

The ability of MD simulations to accurately reflect the real-life properties of a system relies on the accurate modelling of – (i) the interactions between the different particles constituting the system, and (ii) the interaction of the system with its surroundings. While the accuracy of the interatomic interactions depends on the choice of potential ($\Phi(\ldots)$), modelling the interaction between the system and its surroundings depends on the equations of motion. Traditional MD, owing to it

CONTACT Puneet Kumar Patra puneet.patra@civil.iitkgp.ac.in
© 2021 Informa UK Limited, trading as Taylor & Francis Group

conserving the total energy, is well suited for modelling isolated systems. However, it falls short for modelling systems that exchange energy with the surroundings and have a constant temperature. Such scenarios occur very commonly in real-life. For example, most real-life experiments are performed in a constant temperature environment, where a continuous energy exchange occurs between the system and the heat reservoir. In order to model these scenarios through MD, the equations of motion (2) need to be supplemented in a manner that continuous energy exchange is permitted, a constant temperature is enforced, and the dynamics is sampled from the Gibbs' distribution. Such alterations to the equations of motion, however, come with the cost of developing appropriate time-integration techniques.

Apart from accurately mimicking real-life experiments at constant temperatures, temperature control in MD is needed for – (i) identifying the equilibrium properties of a system, (ii) calculating the transport characteristics of systems using Green-Kubo relations or by subjecting the system to dissipative fields, (iii) understanding temperature-dependent mechanical properties of materials, (iv) creating amorphous systems based on high-temperature quenching, and (v) extracting energy from a system on which external work is performed, etc. In fact, temperature control in MD is essential for studying non-equilibrium situations due to the lack of sound theoretical understanding of non-equilibrium statistical thermodynamics.

Initial attempts at developing temperature control algorithms revolved around controlling the kinetic temperature of the system, and until as recently as the early part of this century, only kinetic temperature based thermostats existed. However, recent advances in statistical mechanics have rendered new ways of defining temperature. The temperature of a system in MD, which used to be invariably kinetic temperature, now can be defined solely in terms of the configurational variables. These advances have prompted the development of different classes of temperature control algorithms, with each algorithm having its own strength and weakness.

In this review, our objective is to provide a comprehensive guide for researchers trying to simulate a system whose (part or whole) temperature is controlled. We briefly describe the applicability of the different temperature control algorithms to different scenarios – both equilibrium and non-equilibrium. Using the pedagogical case of a single harmonic oscillator (SHO), under both equilibrium and non-equilibrium conditions, we demonstrate the dynamical behaviour of the different thermostats. Subsequently, we use a one-dimensional Φ^4 chain and a two-dimensional soft-sphere system to compute the transport properties from the thermostatted non-equilibrium MD simulations. The scope of this work is limited to deterministic thermostats. This review is organised as follows: in the next section, we discuss the thermodynamic definition of temperature, which is followed by the properties of a good thermostat. We, subsequently, discuss the different ways of defining operational temperature in MD simulations – kinetic, generalised, configurational, and Rugh's – and algorithms for their control. The case studies, involving SHOs, the Φ^4 chain and the two dimensional soft-sphere system, follow next. The review ends with a set of open-ended questions, whose answers, once obtained, may further enrich thermostatted dynamics.

2. Thermodynamic definition of temperature

Theoretically, the concept of temperature goes beyond mere perception of the degree of hotness or coldness of a body. Instead, it has a solid mathematical background. The idea of temperature begins with the Zeroth Law of thermodynamics. The Zeroth Law enables us to define a class of equivalence relations that is symmetric, reflexive, and transitive [3]. These equivalence relations are isotherms, each of which is associated with an empirical variable called temperature. However, the Zeroth Law in itself is not sufficient to identify the relative degree of hotness. For this purpose, we need both the First Law and the Second Law of thermodynamics.

The First Law enables us to define heat energy in terms of the conservation of total energy. In a closed system, the sum of the change in internal energy and thermodynamic work done by the system equals heat energy supplied to the system:

$$\delta Q = \mathrm{d}U + \delta W = \mathrm{d}U + P\,\mathrm{d}V, \tag{4}$$

where δQ is the heat energy supplied to the system, $\mathrm{d}U$ is the change in the internal energy of the system, and δW is the work done by the system which can be expressed in terms of the pressure, P, and the change in volume, $\mathrm{d}V$.

The Second Law helps in identifying the relative hotness of two bodies in terms of the spontaneous flow of heat energy between them. For a reversible process (necessarily in equilibrium), one can replace the LHS of (4) and rewrite it as:

$$T\,\mathrm{d}S = \mathrm{d}U + P\,\mathrm{d}V, \tag{5}$$

where, T = temperature of the system, and $\mathrm{d}S$ is the change in entropy of the system. All three laws combined together give the thermodynamic definition of temperature,

$$\frac{1}{T} = \left(\frac{\partial S}{\partial U}\right)_V \tag{6}$$

One can understand temperature as the change in the internal energy of a system for a unit change in its entropy at constant volume [4]. Interestingly, the temperature may also be viewed as an integrating factor that converts the path differential variable δQ to the total differential variable dS. Both these interpretations do not preclude the concept of negative temperature [5].

The concept of thermodynamic temperature may be understood in other ways as well. Consider Jaynes' framework of statistical mechanics [6,7], where one maximises the Shannon's entropy functional [8],

$$C = \int f(\mathbf{\Gamma}) \log\left(f(\mathbf{\Gamma})\right) \mathrm{d}\mathbf{\Gamma}, \tag{7}$$

subjected to the constraints imposed by the physics of the problem. For example, there are two constraints in a canonical

ensemble – the phase-averaged energy constraint, $\langle H \rangle = E$, and the normalisation constraint, $\int f(\mathbf{\Gamma})\,\mathrm{d}\Gamma = 1$. The least biased distribution for the canonical ensemble can be found by maximising:

$$C = \int f(\mathbf{\Gamma}) \log\left(f(\mathbf{\Gamma})\right) \mathrm{d}\mathbf{\Gamma} - \lambda_0 \left(\int f(\mathbf{\Gamma})\,\mathrm{d}\Gamma - 1 \right) - \lambda_1 \left(\int H(\mathbf{\Gamma}) f(\mathbf{\Gamma})\,\mathrm{d}\mathbf{\Gamma} - E \right), \tag{8}$$

where, λ_0 and λ_1 are the Lagrange multipliers associated with the normalisation constraint and the energy constraint, respectively. It is straightforward to show that the least biased distribution is the canonical distribution, with $\lambda_1 = \beta = 1/k_B T$ [3]. Here, k_B is the Boltzmann constant. Thus, the temperature of a system may be identified as the inverse of the Lagrange multiplier associated with the energy constraint.

From an operational perspective, measurement and control of thermodynamic temperature are difficult, both in equilibrium and non-equilibrium. This is because the computation of Gibbs' entropy in equilibrium comprises a $6N$ dimensional integral. The situation is more problematic in non-equilibrium, where the meaning of S itself remains an open question. As a result, in MD we rarely use thermodynamic temperature [9]. Instead, other definitions of temperature, some of which we describe later, are used. We emphasise that these different definitions are essentially phase-averaged quantities that are *equal* to the thermodynamic temperature in equilibrium. In non-equilibrium problems, whether these phase-averaged quantities can be ascribed the meaning 'thermodynamic temperature' is a question open to debate. However, for operational reasons we still treat them synonymously with thermodynamic temperature.

3. Properties of a good deterministic thermostat

The role of a good deterministic thermostat goes beyond just controlling the temperature of the system. So, what makes a deterministic thermostat good? Some of the properties are listed below:

(1) *Time-reversibility*: Consider a deterministic system which starts at the microstate $(\mathbf{x_0}, \mathbf{p_0})$, and evolves to the microstate $(\mathbf{x_\tau}, \mathbf{p_\tau})$ in time τ. Hamiltonian mechanics suggests that if $\mathbf{p_\tau}$ is reversed instantaneously i.e. $\mathbf{p_\tau} \to -\mathbf{p_\tau}$ and the dynamics proceeds for a time duration of τ, the initial microstate with reversed momenta i.e. $(\mathbf{x_0}, -\mathbf{p_0})$, is obtained. Alternatively, if the system starts from the microstate $(\mathbf{x_\tau}, \mathbf{p_\tau})$ and proceeds backward in time for a time duration of τ, the initial microstate is reached. Time reversibility of the dynamics is important because some of the fundamental properties of dynamical systems, such as conservation laws, depend on it [10]. The arrow of time does not have any naturally preferred direction when it comes to the fundamental interactions, and all equations of motion in classical mechanics are time-reversible. Thus, the equations of motion for a deterministic thermostat *should* obey similar time-reversal symmetry to be at the same platform as the other equations encountered in physics.

(2) *Ergodicity*: MD simulations are typically performed with one sample-path, which begins from a specific set of initial conditions. The properties measured from MD simulations are, as a result, time-averaged quantities obtained over the single sampled path. Macroscopic averages, on the other hand, are based on the phase-space averages of dynamical observables [11]. The link between the time-averages and the phase-averages is provided by the 'ergodic hypothesis', which states that a phase-averaged variable is the same as its time-averaged counterpart. In essence, ergodicity of the dynamics is a prerequisite for obtaining statistical-mechanical properties from a single run of MD simulation. Throughout this work, we use Ehrenfests' '*quasiergodicity*' equivalently with the traditional ergodicity. (Quasi)ergodicity says that a trajectory initiating from any microstate within the accessible phase-space must eventually come arbitrary close to all the microstates that lie within the accessible region [12]. In the context of MD simulations, this implies that the phase-space trajectory must visit the accessible phase space in a frequency commensurate with the theoretical phase-space probability distribution.

The ergodic hypothesis has been proved theoretically only for a handful of systems like hard billiard balls [13] and Lorentz gas [14]. One usually employs numerical techniques to determine if the dynamics is ergodic. It has been customary to study the ergodic characteristics of thermostatted dynamics using an SHO [15–18] due to the oscillator's 'stiff' nature and simplicity. To the best of our knowledge, no watertight proof of ergodicity exists for any thermostatted dynamics. In larger systems, comprising hundreds of thousands of degrees of freedom, the (non)ergodicity of dynamics takes a back seat owing to the large Poincaré recurrence time, which often is greater than the age of the universe [19]. Thus, although ideally, we *need* algorithms that impart ergodicity to the dynamics, the effect of non-ergodicity becomes progressively less important as the system size increases.

There are two ways of ascertaining ergodicity numerically. Both the approaches are briefly described, and the interested readers are referred to [20,21] for a more comprehensive treatment. Note that in both approaches, we deal with a SHO.

Dynamical Systems Approach: Non-ergodicity implies the partitioning of the phase-space into two (or more) non-communicating regions. So, when the dynamics of a thermostatted SHO is limited to a (hyper-)torus for one or more initial conditions (except perhaps those that form a set of zero-measure), the thermostatted dynamics is non-ergodic. For a multidimensional phase-space flow, as is the case with thermostatted SHOs, this can be assessed by studying the Lyapunov spectra of the dynamics [22]. A $d-$dimensional flow is associated with d Lyapunov exponents, which are ordered: $L_1 > L_2 > \cdots > L_{d-1} > L_d$. The sum of these exponents describes the deformation of an infinitesimal hypercube in the $d-$dimensional space describing the motion. L_1 gives

the time-averaged rate of separation of two neighbouring trajectories. $L_1 + L_2$ gives the rate of separation of the area defined by three neighbouring trajectories. Similarly, $L_1 + L_2 + L_3$ describes the separation rate of volume, and so on. The pre-deformation infinitesimal hypervolume $\delta V(0)$ with the post-deformation hypervolume $\delta V(t)$ may be related as:

$$\delta V(t) = \delta V(0) e^{(L_1+L_2+\cdots+L_{d-1}+L_d)t} \tag{9}$$

In equilibrium, $\sum\langle L_i\rangle = 0$, i.e. there is no change in phase-space volume in an averaged sense, and $\langle L_1 + L_d\rangle = \langle L_2 + L_{d-1}\rangle = \ldots = 0$, i.e. the Lyapunov exponents are conjugately paired. To ascertain the ergodic characteristics, Lyapunov spectra corresponding to millions of initial conditions need to be found. For non-ergodic dynamics, at least one initial condition yields a (hyper-)torus for which all the Lyapunov exponents are statistically insignificant from zero.

Statistical Approach: Consider the Maxwell-Boltzmann distribution. For an SHO of unit mass and stiffness, the Maxwell-Boltzmann distribution reduces to a product of two independent normal distributions:

$$f(x, p) = \frac{1}{Z}\left[\exp\left(-\frac{\beta_0}{2}x^2\right)\exp\left(-\frac{\beta_0}{2}p^2\right)\right] \tag{10}$$

In the presence of thermostat variables $(\eta_1, \eta_2, \ldots, \eta_n)$, the distribution function gets augmented by additional terms. However, the conditional distribution of oscillator's position and momentum variables still remains jointly normal i.e.

$$f(x, p|\eta_1 = \eta_{1,0}, \eta_2 = \eta_{2,0}, \ldots, \eta_n = \eta_{n,0}) = \frac{1}{Z'}\left[\exp\left(-\frac{\beta_0}{2}x^2\right)\exp\left(-\frac{\beta_0}{2}p^2\right)\right] \tag{11}$$

The statistical approach of ascertaining ergodicity looks at this conditional joint distribution of position and momentum to assess if the dynamics samples the phase-space following the Maxwell-Boltzmann distribution. Any deviation from normality is an indicator of non-ergodicity. Numerically, this implies finding the joint probability distribution of position and momentum in a Poincaré section defined by $\eta_1 = \eta_{1,0}$, $\eta_2 = \eta_{2,0}$, $\ldots$, $\eta_n = \eta_{n,0}$, and performing a test for normality.

It is important to note that the marginal distributions of position and velocity are often incapable of capturing the deviation from normality. This is exemplified next. Consider a four-dimensional space filled with 10 million random samples drawn from the independent standard normal vectors (n_1, n_2, n_3, n_4). Let a small hole be embedded in this 4-D space by deleting the points that lie within the hyper-sphere $n_1^2 + n_2^2 + n_3^2 + n_4^2 \leq 0.0625$. Clearly, having lost all probability content around the origin of the 4-d space, the remaining points would no longer satisfy a joint normal density function. However, the phase-space plot projected on to $n_3 = 0$, $n_4 = 0$ plane is devoid any empty space (see Figure 1(a)), and the marginal distributions of n_1 and n_2 agree well with a standard normal distribution (see Figures 1(b,c)). The first three even marginal and joint moments also agree well with the standard normal distribution: $\langle n_1^2\rangle = 1.000$, $\langle n_1^4\rangle = 3.000$, $\langle n_1^6\rangle = 15.007$, $\langle n_2^2\rangle = 0.999$, $\langle n_2^4\rangle = 2.999$, $\langle n_2^6\rangle = 14.992$, $\langle n_1^2 n_2^2\rangle = 0.999$, $\langle n_1^4 n_2^4\rangle = 9.003$ and $\langle n_1^6 n_2^6\rangle = 227.496$. Thus, one needs to check ergodicity using conditional joint distributions rather than marginal distributions.

(3) *Conformity with the Laws of Thermodynamics*: Being mathematical counterparts of the real-life thermal reservoirs, the thermostat algorithms *must* satisfy the different laws of thermodynamics. Take the Zeroth Law of thermodynamics, for example, which says that if two bodies are in mutual thermal equilibrium with a third body, then the two bodies are in thermal equilibrium with each other. Now, consider a system in thermal equilibrium with known macroscopic properties. If this system is coupled with a thermostat (algorithm) at the same temperature, then as per the Zeroth Law, the macroscopic properties of the system remain time-invariant. Going one step further, if the system is coupled with more than one thermostat, the properties of not only the system but the individual thermostats also remain time-invariant. This idea is

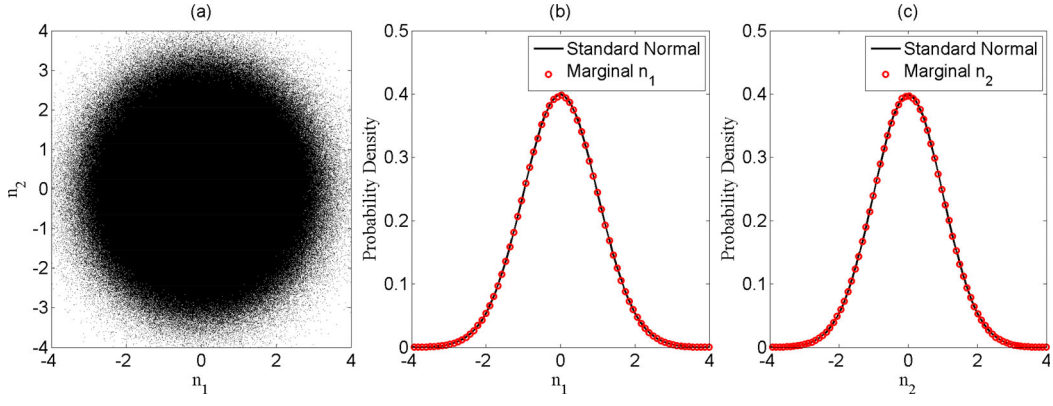

Figure 1. (Colour online) The inability of projected variables $n_1 - n_2$ to capture the 4-dimensional hole of radius 0.25 forcefully embedded within a 4-dimensional joint standard normal. (a) Projected values of $n_1 - n_2$ onto the $n_3 = 0$, $n_4 = 0$ plane. (b) Marginal distribution of n_1 and (c) marginal distribution of n_2. No difference in marginal distributions from that of standard normal can be observed.

central to testing if a thermostat algorithm satisfies the Zeroth Law: an SHO is simultaneously coupled with two thermostats kept at the same temperature. The resulting equations of motion are solved, and the phase-space of the oscillator is analysed along with that of the thermostat. The Zeroth Law is not satisfied if: (i) the temperature of any of the thermostats differ from that of the system or with each other, (ii) there is a heat flow within the system, or (iii) the time-averaged phase-space compression, which is defined as,

$$\langle \Lambda \rangle_t = \frac{1}{\tau} \frac{\partial \dot{\mathbf{\Gamma}}}{\partial \mathbf{\Gamma}}, \tag{12}$$

is not equal to zero. Here, τ represents the time, and $\mathbf{\Gamma} \equiv (x, p, \eta_1, \eta_2, \ldots, \eta_k)$ denotes the extended phase-space, with η_is as the thermostat variables.

The Second Law, on the other hand, demands heat to flow from a thermostat at a higher temperature to a thermostat at a lower temperature spontaneously. In essence, if one end of a system is thermostatted at a higher temperature and the other end at a lower temperature, then a spontaneous heat flow *must* occur between the hotter and the colder thermostats. Thermostats unable to engineer such a heat flow fail to satisfy the Second Law, and hence, are not suitable for MD simulations. Apart from the ability to ensure heat flow, the time-averaged phase-space compression, defined by (12), must be non-zero. In order to check if a thermostat satisfies the Second Law, we take an SHO and subject it to a position-dependent temperature field

$$k_B T(x) = 1 + \epsilon \tanh(x), \tag{13}$$

by coupling it with a thermostat. Here, ε denotes the strength of non-linearity. For $\epsilon \neq 0$, this becomes a non-equilibrium problem, with heat flow and phase-space compression.

(4) *Autonomous and Easy Implementation*: The equations of motion corresponding to the deterministic thermostats must be autonomous, i.e. they should not have an explicit dependence on time. An explicit dependence on time makes the equations lose their time-invariance characteristic, which is a prerequisite for equilibrium. Lastly, the equations of motion must be easy to implement, not be stiff, and simple to solve using existing numerical techniques.

4. Kinetic temperature and its control

In MD simulations, the temperature used to be invariably expressed in terms of the kinetic variables. The kinetic definition of temperature owes its origins to the kinetic theory of gases. Consider an isolated system comprising ideal gas particles that are confined to move within a container. The particles are assumed to be rigid and collide elastically with each other and with the walls. A quick comparison of the pressure exerted by the particles on the wall surface with the ideal gas equation of state reveals that the kinetic temperature [23], T_k, is:

$$\frac{3}{2} k_B T_k = \left\langle \frac{p_i^2}{2m} \right\rangle. \tag{14}$$

Here, $\langle \ldots \rangle$ denotes the phase-averaged quantity. Unlike thermodynamic temperature, the expression of T_k is easy to compute and control in a computer simulation without expending too many computational resources. If the system is in equilibrium and is isotropic, as is the case with an ideal gas or a system without any directional dependence, one can employ equipartition theorem to show that, in an averaged sense, each kinetic energy component is equal to the other and to the thermodynamic temperature i.e.

$$\frac{1}{2} k_B T_k = \left\langle \frac{p_{i,x}^2}{2m} \right\rangle = \left\langle \frac{p_{i,y}^2}{2m} \right\rangle = \left\langle \frac{p_{i,z}^2}{2m} \right\rangle \tag{15}$$

Alternatively, T_k may be derived from the canonical probability distribution function, wherein the phase space is sampled according to the Maxwell-Boltzmann distribution:

$$f(\mathbf{x}, \mathbf{p}) = \frac{1}{Z} \exp\left(-\beta \Phi(\mathbf{x}) - \beta \left[\sum_{i=1}^{3N} p_i^2 / 2m \right] \right). \tag{16}$$

Here, Z is the partition function and $\beta = (k_B T)^{-1}$. Equations (14) and (15) may be obtained by relating, $1/\beta$, the variance of the Maxwell-Boltzmann distribution with the momentum variables.

From a statistical perspective, when a system is in thermal equilibrium with a reservoir, *all* moments of the momentum distribution must agree with the kinetic temperature of the system. This statistical nature of the momentum variables may be exploited to obtain higher-order measures of T_k, as often, it has been observed that the control of the second-moment based T_k alone is insufficient for effectively thermalising small-scale systems such as SHOs. With this in mind, higher-order moments of kinetic temperature – $T_{k,2}$, the kinetic temperature calculated from the fourth moment of velocity distribution and $T_{k,3}$, the kinetic temperature calculated from the sixth moment of velocity distribution – may be calculated as:

$$k_B T_{k,2} = \sqrt{\frac{\langle p_i^4 \rangle}{3m^2}}, \quad k_B T_{k,3} = \sqrt{[3]} \frac{\langle p_i^6 \rangle}{15 m^3}. \tag{17}$$

An unconventional route to kinetic temperature is from the viewpoint of the kinetic energy of the system – as particle velocities are normally distributed, the kinetic energy, K, follows a χ^2 distribution. Based on this argument, T_k shown in equation (14) represents the mean of the χ^2 distribution. Although T_k calculated from the first even order moment of momentum distribution and the first moment of kinetic energy distribution agree with each other, the second-order kinetic temperature obtained from kinetic energy distribution, $T_{K,2}$, is different from that of $T_{k,2}$:

$$k_B T_{K,2} = \frac{\langle 4K^2 \rangle}{\langle 2K(N+2) \rangle} \tag{18}$$

It is important to note that all expressions of kinetic

temperature written so far apply only to the translation motion of the individual particles. These expressions require modification if there is a centre of mass translation or if rotational and internal degrees of freedom are present [24].

The kinetic temperature control algorithms may be divided into three categories – temperature constraining algorithms (Velocity Rescaling and Gaussian isokinetic thermostat), temperature control through weak coupling (Berendsen thermostat) and temperature control through extended system (Nosé, Nosé-Hoover, Martyna-Klein-Tuckerman, Hoover-Holian and Campisi-Zhan-Talkner-Hängii thermostats). We now discuss these categories.

4.1. Temperature constraining algorithms

The primary idea behind these algorithms is to *constrain* the instantaneous kinetic temperature, Equation (14), to the desired value. The constraining may be performed in an adhoc manner (Velocity Rescaling and Berendsen thermostats) or through a more physics based approach (Gaussian Isokinetic thermostat). Constraining the temperature reduces the independent degrees of freedom of the system by one, and removes fluctuations in temperature. These algorithms do not generate a canonical distribution in momentum variables, however, a canonical distribution is generated for the configurational variables [25]. Note that the absence of temperature fluctuations could result in inaccurate solutions in typical systems employed in MD simulations.

4.1.1. Velocity rescaling and berendsen thermostats

Velocity rescaling is possibly the simplest of all temperature control algorithms. As the name suggests, the instantaneous velocities of the particles are rescaled in an ad-hoc manner such that the desired temperature, T_0, is obtained [26]. For a $d-$dimensional system, T_0 is related to the desired kinetic energy, K_0, as:

$$T_0 = \frac{2}{\mathrm{d}Nk_B} K_0. \tag{19}$$

Let, at any time t, the instantaneous kinetic energy, K_t, be given by: $K_t = \sum p_i^2/2m$. The corresponding instantaneous kinetic temperature, T_t, is $T_t = 2K_t/(k_B dN)$. Evidently, if the instantaneous velocities of each particle are scaled by a factor α, where,

$$\alpha = \sqrt{\frac{K_0}{K_t}} \tag{20}$$

the instantaneous temperature of the system is forced at T_0. The rescaling may be performed after every few steps.

The sampled ensemble is not canonical in momentum variables. However, in massive systems, this algorithm may provide satisfactory results due to the equivalence of different ensembles in the thermodynamic limit [27]. Apart from the inability to sample the dynamics correctly, this algorithm is not physics preserving [25], and does not follow any of the properties of a good thermostat discussed before. The sampled space and the temperature fluctuations depend on the frequency of rescaling. For example, if the rescaling is done every time step, then the fluctuations in temperature are zero. Because of these reasons, this simple algorithm is typically not used these days. However, a simple modification can remove some of the drawbacks. Rather than treating K_0 as a hard equality constraint, if one treats it as a soft constraint, where at each rescaling step it is sampled from an appropriate χ^2 distribution [28], some of the problems are resolved.

The Berendsen thermostat [29] is a weaker form of the velocity rescaling algorithm. In this, the velocities are rescaled at each time step so that the rate of change of temperature is proportional to the instantaneous difference between the desired temperature and the actual temperature:

$$\frac{\mathrm{d}T(t)}{\mathrm{d}t} = \frac{1}{\tau}[T_0 - T_t], \tag{21}$$

where, τ is the time parameter that determines the (exponential) rate at which the actual temperature decays to the desired temperature. The temperature of the system after one iteration is: $T_t + \Delta T = T_t + \frac{\Delta t}{\tau}(T_0 - T_t)$, from which the velocity rescaling factor may be calculated:

$$\alpha' = \sqrt{\frac{T_t + \Delta T}{T_t}}. \tag{22}$$

Like the Velocity rescaling thermostat, the Berendsen thermostat does not sample the dynamics from a canonical distribution. In some cases, the Berendsen thermostat results in the unphysical flying ice cube effect, wherein the energy of the high-frequency normal modes is funnelled into the low-frequency modes, and hence, it is advised to avoid this thermostat [30].

4.1.2. Gaussian isokinetic thermostat

Amongst the first physics-preserving deterministic thermostats, the Gaussian isokinetic thermostat (GIK) was simultaneously developed by Hoover [31] and Evans [32–34]. In here, the kinetic energy (and thereby, the kinetic temperature) is controlled through the non-holonomic constraint [35,36]:

$$g(x_i, \dot{x}_i, t) = \sum_{i=1}^{3N} \frac{1}{2} m\dot{x}_i^2 - \frac{3}{2} Nk_B T_0 = 0. \tag{23}$$

Being a hard equality constraint, the kinetic energy of the system remains equal to $3/2Nk_BT_0$ at all times. The equations of motion are obtained from the Gauss' principle of least constraint, which states that the true trajectory of a constrained system is the one that minimises the difference between the true acceleration and the unconstrained acceleration of the constituent particles in a least-squares manner [35]:

$$M = \frac{1}{2} \sum_{i=1}^{3N} m\left(\ddot{x}_i - \frac{F_i}{m}\right). \tag{24}$$

Here, $\ddot{x}_i$ is the true acceleration of the i^{th} particle and $\frac{F_i}{m}$ is its unconstrained acceleration. The constraint equation (23) is brought to the acceleration space: $G(\dot{x}_i, \ddot{x}_i, t) = \sum_{i=1}^{3N} m\dot{x}_i.\ddot{x}_i = 0$, and M of Equation (24) is minimised subjected to G through the Lagrange multiplier, λ. The equations

of motion become:

$$m\ddot{x}_i = F_i - \lambda m\dot{x}_i. \tag{25}$$

λ may be obtained by substituting equation (25) in the differential constraint, G:

$$\lambda = \frac{\sum F_i\dot{x}_i}{\sum m\dot{x}_i^2} = \frac{\sum F_i p_i}{\sum p_i^2}. \tag{26}$$

Notice that the equations of motion do not explicitly account for T_0. The information on T_0 goes into the dynamics from the initial description of the system – the initial kinetic energy of the system equals $3/2Nk_BT_0$. An incorrect choice of the initial conditions results in the system being thermalised at an incorrect value. Equation (25) bears similarity to a damped system, where λ acts like the damping coefficient. However, in the GIK thermostat, the magnitude and the sign of λ depends on the instantaneous value of equation (26): $\lambda > 0 (< 0)$ indicates that the reservoir extracts (supplies) heat energy from (to) the system. The pseudo-energy which is a constant of motion is given by:

$$E_{GIK} = \Phi(\mathbf{x}) + \sum\frac{p_i^2}{2m} + \int_0^t \sum F_i p_i \, \mathrm{d}t \tag{27}$$

Equations of motion of the GIK thermostat can also be derived using a Hamiltonian formulation [37]. For simplicity, consider the case where $k_BT_0 = 1$ and m=1. Let the Hamiltonian, H_{GIK}, be given by:

$$H_{\mathrm{GIK}}(x_i, \pi_i, t') = \frac{1}{2}e^{[(\gamma+1)\Phi]}\sum_{i=1}^{3N}\pi_i^2 - \frac{1}{2}e^{[(\gamma-1)\Phi]}, \tag{28}$$

where Φ is the potential energy, π_i is the momentum conjugate to x_i and is different from the real momentum p_i, t' is the Hamiltonian time, which is different from the real time t, and γ is an arbitrary multiplier. Applying Hamilton's equations provides:

$$\begin{aligned}\frac{\mathrm{d}x_i}{\mathrm{d}t'} &= \frac{\partial H_{\mathrm{GIK}}}{\partial \pi_i} = e^{[(\gamma+1)\Phi]}\pi_i \\ \frac{\mathrm{d}\pi_i}{\mathrm{d}t'} &= \frac{-\partial H_{\mathrm{GIK}}}{\partial x_i} = \frac{-1}{2}\frac{\partial\Phi}{\partial x_i}e^{[(\gamma-1)\Phi]} \\ &\quad \times\left[(\gamma+1)e^{(2\Phi)}\sum_{i=1}^{3N}\pi_i^2 - (\gamma-1)\right].\end{aligned} \tag{29}$$

Equations (25) and (26) can be obtained from Equation (29), if the following relation is imposed on the Hamiltonian variables and the real-time variables:

$$\frac{\mathrm{d}t}{\mathrm{d}t'} = \exp[-\gamma\Phi], \quad p_i = \exp[\Phi]\pi_i. \tag{30}$$

The Hamiltonian formulation enables the study of GIK thermostatted dynamics within the framework of Hamiltonian mechanics, including conservation of phase-space volume and its symplectic structure. The GIK thermostatted dynamics is a part of the $\mu-$ thermostat family, under the special condition of $\mu = 1$ [38], and is unique amongst the different $\mu-$ thermostat candidates as it is the only one from the family – (i) for which the conjugate pairing rule holds, and (ii) which generates an equilibrium state.

The GIK thermostat samples the configurational space canonically and the momentum space microcanonically. Let f_{GIK} be the distribution function generated by the GIK equations of motion, then the Liouville's equation becomes:

$$\frac{\mathrm{d}f_{GIK}}{\mathrm{d}t} = -f_{GIK}\frac{\partial}{\partial\mathbf{\Gamma}}.\dot{\mathbf{\Gamma}} = f_{GIK}\sum_{i=1}^{N}\frac{\partial}{\partial\mathbf{p}_i}.(\lambda\mathbf{p}_i), \tag{31}$$

where, $\mathbf{\Gamma} = (\mathbf{x}, \mathbf{p})$ denotes the phase-space variables. Neglecting the $3N$ terms obtained from the derivative $\mathbf{p}_i.\partial\lambda/\partial\mathbf{p}_i = -\lambda$, Equation (31) may be simplified to:

$$\frac{\mathrm{d}f_{GIK}}{\mathrm{d}t} = 3N\lambda f_{GIK} = \frac{-3N}{2K}f_{GIK}\dot{\mathbf{\Phi}}, \tag{32}$$

which upon integration in time yields:

$$f_{GIK}(\mathbf{\Gamma}) = \frac{\exp[-\beta\mathbf{\Phi}]\delta(K - K_0)}{\int(\exp[-\beta\mathbf{\Phi}]\delta(K - K_0))\,\mathrm{d}\mathbf{\Gamma}}. \tag{33}$$

Consequently, a single GIK trajectory *cannot* sample the dynamics canonically even if it is ergodic. It is easy to check that the phase-space compression factor, $\Lambda = \frac{\partial}{\partial\mathbf{\Gamma}}.\dot{\mathbf{\Gamma}} \neq 0$, but in absence of any dissipative field, $\langle\Lambda\rangle = 0$ as $\langle\dot{\mathbf{\Phi}}\rangle = 0$ in equilibrium. The instantaneous rate at which the GIK thermostat exchanges heat with the system is:

$$\dot{Q}_{GIK}(t) = \frac{\mathrm{d}}{\mathrm{d}t}[K(t) + \mathbf{\Phi}(t)] = -\lambda(t)\sum_{i=1}^{N}\frac{\mathbf{p}_i^2}{m_i}. \tag{34}$$

It has been observed that in the long-time limit, the temperature drifts away from its desired value. The solution lies in adding a proportional feedback term [39] through a modified form of the Lagrange multiplier:

$$\lambda' = \lambda + c\left[\frac{\sum p_i^2/m - 3Nk_BT_0}{3Nk_BT_0}\right], \tag{35}$$

where, c is the weighting term, which typically varies between 0.1 and 10. However, this correction introduces irreversibility into the dynamics.

For non-equilibrium problems, the GIK thermostat has been extensively used for studying three-dimensional Couette flow [40–40], as the peculiar kinetic energy can be made a constant of motion:

$$\begin{aligned}\dot{\mathbf{r}}_i &= \tfrac{\mathbf{p}_i}{m} + n_x\dot{\gamma}y_i \\ \dot{\mathbf{p}}_i &= \mathbf{F}_i - n_x\dot{\gamma}p_{y,i} - \lambda\mathbf{p}_i \\ \lambda &= \frac{\sum_{i=1}^{N}\mathbf{F}_i.\mathbf{p}_i - \dot{\gamma}p_{x,i}p_{y,i}}{\sum_{i=1}^{N}\mathbf{p}_i.\mathbf{p}_i}\end{aligned} \tag{36}$$

Here, $\mathbf{r} \equiv (x, y, z)$ and $\mathbf{p} \equiv (p_x, p_y, p_z)$ denote the position and momentum of the particles, respectively, n_x is a unit vector in the $x-$direction and $\dot{\gamma}$ is the shear rate. Evidently, Couette flow is treated as a mechanical perturbation by writing the equations of motion in terms of peculiar momenta [43]. However, the correctness of such enforcement has been questioned [44], and at large strain rates, a string phase is formed in the system, which will be discussed in the case study.

4.2. Thermostats based on the extended system method

In the extended system method, the temperature is controlled by coupling the physical system to a 'hypothetical' heat bath. The heat bath is represented by additional degrees of freedom. While the total energy of extended system, comprising the physical system and the heat bath, remains constant, the total energy of the physical system fluctuates [45]. Nosé did the pioneering work on the extended system thermostats [46,47], although the idea of extended system can be traced back to Andersen [48] for his constant pressure method. Nosé introduced two types of variables – real variables that represent the dynamics of the physical system in real time, and time-scaled variables that represent the virtual evolution of the system in Hamiltonian time. Subsequently, Hoover [49] proposed a simplification to the Nosé's equations of motion, which is now known as the Nosé-Hoover thermostat. While Nosé's original formulation and Hoover's modification satisfy several properties of a good thermostat, when coupled with very small systems, the dynamics is non-ergodic. This issue may be tackled through the Nosé-Hoover chain thermostat [50,51] and the kinetic-moment based thermostat [52], all of which we describe in this section.

Typically, the thermostats based on the extended system method can be developed in two separate ways:

(1) Develop a Lagrangian or a Hamiltonian for the extended system in such a manner that when the heat bath variables are integrated out, the dynamics of the physical system is sampled from a canonical distribution. This method was adopted by Nosé [45] and Campisi et. al [53,54] to develop their thermostats.
(2) Alternatively, one can use the Guessing Method of Holian and Hoover, which was further generalised by Bauer, Bulgac and Kusnezov [16,55]. Assuming an arbitrary coupling between the physical system and the heat baths – denoted by $h_1(\xi)$ and $h_2(\eta)$, the position and the momentum evolution equations may be written as:

$$\begin{aligned}\dot{x}_i &= \frac{p_i}{m} - h_1(\xi)C_i(x_i,\ p_i)\\ \dot{p}_i &= -\frac{\partial\Phi}{\partial x_i} - h_2(\eta)D_i(x_i,\ p_i),\end{aligned} \tag{37}$$

where, $C_i(x_i, p_i)$ and $D_i(x_i, p_i)$ are arbitrary phase functions. The temporal evolution of the heat bath variables – ξ and η, are obtained by solving the extended phase-space Liouville's equation:

$$\frac{\partial f_{\rm ex}}{\partial t} + \frac{\partial f_{\rm ex}}{\partial \mathbf{\Gamma}}.\dot{\mathbf{\Gamma}} = -f_{\rm ex}\frac{\partial \dot{\mathbf{\Gamma}}}{\partial \mathbf{\Gamma}}, \tag{38}$$

where the extended phase-space, $\mathbf{\Gamma} = (\mathbf{x}, \mathbf{p}, \xi, \eta)$ comprises $6N+2$ dimensions, and $f_{\rm ex}(\mathbf{\Gamma})$ is the extended phase-space distribution function:

$$f_{\rm ex}(\mathbf{\Gamma}) = \frac{1}{Z'}\exp\left[-\beta\left(H + \frac{g_1(\xi)}{Q_\xi} + \frac{g_2(\eta)}{Q_\xi}\right)\right] \tag{39}$$

Under the assumptions that the heat bath variables evolve self-consistently $(\partial g_1(\xi)/\partial\xi = h_1,\ \partial g_2(\eta)/\partial\eta = h_2)$ and are independent of their time derivative $(\partial\dot{\xi}/\partial\xi = \partial\dot{\eta}/\partial\eta = 0)$, the evolution equations of the heat bath variables are given by:

$$\begin{aligned}\dot{\eta} &= Q_\eta\sum_{i=1}^{3N}\left[\frac{p_i}{m}D_i(x_i,\ p_i) - k_BT_0\frac{\partial D_i(x_i,\ p_i)}{\partial p_i}\right]\\ \dot{\xi} &= Q_\xi\sum_{i=1}^{3N}\left[\frac{\partial\Phi}{\partial x_i}C_i(x_i,\ p_i) - k_BT_0\frac{\partial C_i(x_i,\ p_i)}{\partial x_i}\right].\end{aligned} \tag{40}$$

Appropriate form of the coupling terms result in a family of thermostats using this method.

We now look at the extended system based thermostats in details.

4.2.1. Nosé thermostat

The strength of the Nosé's approach lies in treating the entire effect of a heat bath through a single variable. The extended system obtained as a result constitutes a micro-canonical ensemble with $6N+1$ degrees of freedom. The physical system, denoted by the variables (x_i, p_i), constantly exchanges heat energy with the heat bath variable, denoted by s with its conjugate momentum denoted by p_s. The variable s may be viewed as a time-scaling factor which relates the real-time evolution with the Hamiltonian (virtual) time evolution of the physical system. The idea of scaling the time arises from the need to provide a feedback mechanism for controlling the momenta, and hence, the temperature. Consider the evolution of the physical system in an incremental time $\mathrm{d}t$, so that $p_i^2 = m(\mathrm{d}x_i/\mathrm{d}t)^2$. If the total kinetic energy is less (more) than $3/2k_BT_0$, then decreasing (increasing) the real time $\mathrm{d}t$ to the virtual time $\mathrm{d}t'$ ensures that the kinetic energy equals $3/2k_BT_0$.

The simplest manner in which the virtual time, t', and the real-time, t, can be related is $\mathrm{d}t = s^{-1}\,\mathrm{d}t'$. As the Hamiltonian time differs from the real-time, the Hamiltonian positions and their conjugate momenta, denoted by x_i' and π_i, respectively, are also different from the real-time positions and momenta; their relation being:

$$x_i = x_i', \quad p_i = \frac{\pi_i}{s}. \tag{41}$$

Let the Lagrangian describing the evolution of the extended system in the Hamiltonian time be chosen as:

$$L_{\rm Nos/e} = \sum_{i=1}^{3N}\frac{m}{2}s^2\dot{x}_i'^2 - \Phi(\mathbf{x}') + \frac{Q_s}{2}\dot{s}^2 - gk_BT_0\log s, \tag{42}$$

then, π_i and p_s', the momenta conjugate to x_i' and s, respectively, are given by:

$$\pi_i = \frac{\partial L_{\rm Nos/e}}{\partial\dot{x}'_i} = ms^2\dot{x}'_i, \quad p_s' = \frac{\partial L_{\rm Nos/e}}{\partial\dot{s}} = Q_s\dot{s}. \tag{43}$$

The overdot notation represents the derivatives with respect to the Hamiltonian time, t'. The term Q_s is a user-controlled parameter, which typically denotes the 'mass' of the thermal reservoir, and g is a constant that denotes the number of degrees of

freedom within the system. Note that $\pi_i \neq m\frac{dx_i'}{dt'}$. Using Legendre transformation, the Hamiltonian corresponding to $L_{\text{Nos/e}}$ can be written as:

$$H_{\text{Nos/e}} = \sum_{i=1}^{3N} \frac{\pi_i^2}{2ms^2} + \Phi(\mathbf{x}') + \frac{p_s'^2}{2Q} + gk_BT_0 \log(s), \tag{44}$$

from which the equations of motion are obtained in the Hamiltonian time:

$$\begin{aligned}
\frac{dx_i'}{dt'} &= \frac{\partial H_{\text{Nos/e}}}{\partial \pi_i} = \frac{\pi_i}{ms^2} \\
\frac{d\pi_i}{dt'} &= -\frac{\partial H_{\text{Nos/e}}}{\partial x_i'} = -\frac{\partial \Phi}{\partial x_i'} \\
\frac{ds}{dt'} &= \frac{\partial H_{\text{Nos/e}}}{\partial p_s'} = \frac{p_s'}{Q_s} \\
\frac{dp_s'}{dt'} &= -\frac{\partial H_{\text{Nos/e}}}{\partial s} = \frac{1}{s}\left[\sum_{i=1}^{3N} \frac{\pi_i^2}{ms^2} - gk_BT_0\right].
\end{aligned} \tag{45}$$

This extended system constitutes a micro-canonical ensemble as it remains isolated from the environment, and all energy exchanges between the system and the reservoir are internal. Consequently, the Hamiltonian represented by equation (44) is a constant of motion. In Hamiltonian time, the phase-space compression factor,

$$\Lambda = \frac{\partial \dot{\mathbf{\Gamma}}}{\partial \mathbf{\Gamma}} = 0. \tag{46}$$

A physical interpretation of $\Lambda = 0$ is that the phase-space probability in a volume element along a phase-space is always conserved.

The real-time evolution of the extended system can be obtained by substituting the relations shown in Equation (41) in Equation (45) along with the relation $p_s = p_s'/s$:

$$\begin{aligned}
\frac{dx_i}{dt} &= \frac{p_i}{m} \\
\frac{dp_i}{dt} &= -\frac{\partial \Phi}{\partial x_i} - \frac{1}{s}\frac{ds}{dt}p_i \\
\frac{ds}{dt} &= \frac{s^2 p_s}{Q_s} \\
\frac{dp_s}{dt} &= \frac{1}{s}\left[\sum_{i=1}^{3N} \frac{p_i^2}{m} - gk_BT_0\right] - \frac{1}{s}\frac{ds}{dt}p_s.
\end{aligned} \tag{47}$$

Unlike that in the Hamiltonian time, in real-time $\Lambda \neq 0$ due to the non canonical nature of the transformation from the virtual to the real variables.

Under the assumption of ergodicity, the real phase-space is sampled as per the Maxwell-Boltzmann distribution, Equation (16), in both real as well as Hamiltonian time. Interested readers are referred to the review paper by Hünenberger [25] for a comprehensive treatment of the derivation. Nosé's extended system formalism was generalised by Jellinek and coworkers [56,57]. By distinguishing between the scaling of the real phase-space variables and the real time, they showed – (i) the time scaling leads to a weighted distribution in the real phase-space, and (ii) there are infinite ways in which the scaling functions can be chosen such that a canonical distribution is sampled.

The Nosé thermostat suffers from two problems – (i) the computation of dynamical properties in real time requires re-weighting (or interpolating) the trajectories in equally spaced time interval, a non-trivial task, and (ii) the Hamiltonian formalism is not applicable to cases where separate temperature control is desired for the different degrees of freedom (such as vibrations, translations and rotations) as each of them has a different relaxation time [58]. These problems can be resolved through the Nosé-Hoover (NH) thermostat.

4.2.2. Nosé-Hoover thermostat

Nosé's equations of motion can be written in the form:

$$\begin{aligned}
\frac{dx_i}{dt} &= \frac{p_i}{m}, \quad \frac{dp_i}{dt} = -\frac{\partial \Phi}{\partial x_i} - \left(\frac{1}{s}\frac{ds}{dt}\right)p_i, \\
\frac{ds}{dt} &= \frac{sp_s'}{Q_s}, \quad \frac{dp_s'}{dt} = \left[\sum_{i=1}^{3N} \frac{p_i^2}{m} - 3Nk_BT_0\right].
\end{aligned} \tag{48}$$

Defining $\eta = p_s'/Q_s$ and $Q_s = Q_\eta$, Hoover [49] simplified these equations to:

$$\begin{aligned}
\frac{dx_i}{dt} &= \frac{p_i}{m}, \quad \frac{dp_i}{dt} = -\frac{\partial \Phi}{\partial x_i} - \eta p_i, \\
\frac{ds}{dt} &= \eta s, \quad \frac{d\eta}{dt} = \frac{1}{Q_\eta}\left[\sum_{i=1}^{3N} \frac{p_i^2}{m} - 3Nk_BT_0\right].
\end{aligned} \tag{49}$$

As the differential equation for s is redundant, the remaining three differential equations are self-sufficient in describing the extended-system dynamics. These three equations constitute the NH thermostat.

The NH equations of motion satisfy the steady-state Liouville's Equation (38) in a comoving frame of reference [59] with $\mathbf{\Gamma} = (\mathbf{x}, \mathbf{p}, \eta)$ and f_{ex} equalling:

$$f_{\text{ex}}(\mathbf{\Gamma}) = \frac{1}{Z'} e^{\left[-\beta\left(\sum_{i=1}^{3N} \frac{p_i^2}{2m} + \Phi(\mathbf{x})\right)\right]} \times e^{\left[-\frac{\beta Q_\eta}{2}\eta^2\right]} \tag{50}$$

The instantaneous phase-space compression factor, $\Lambda = [\frac{\partial \dot{\mathbf{x}}}{\partial \mathbf{x}} + \frac{\partial \dot{\mathbf{p}}}{\partial \mathbf{p}} + \frac{\partial \dot{\eta}}{\partial \eta}] = -3N\eta \neq 0$, which suggests that the phase-space probability is not conserved along a phase-space trajectory. However, since in an averaged sense, $\langle \eta \rangle = 0$, $\langle \Lambda \rangle = 0$ as well. The NH equations of motion bear similarity to the GIK thermostat, the difference being the dynamic evolution of η.

The Guessing Method discussed previously can be used to derive the NH equations of motion. Starting with the Equation (37) under the coupling $h_1(\xi) = C_i(x_i, p_i) = 0$, $h_2(\eta) = \eta$ and $D_i(x_i, p_i) = p_i$, one ends up with Equation (49) if the extended phase-space distribution is chosen according to the Equation (50). The NH equations of motion may also be obtained from a Hamiltonian described by Dettmann and Morriss [60]:

$$H_{\text{D\&M}} \equiv sH_{\text{Nos/e}} \equiv 0 \tag{51}$$

This Hamiltonian omits the time-scaling variable used in the Nosé's Hamiltonian. Bond and coworkers developed a more formal approach, the Nosé-Poincaré method, to come up with the same Hamiltonian [61]. Note that for some non-equilibrium problems of one-dimensional oscillators, the

traditional Nosé-Hoover equations differ [62] from those obtained using equation (51).

For the NH equations, the pseudo energy, defined by:

$$E_{NH} = \sum_{i=1}^{3N} \frac{p_i^2}{2m} + \Phi(\mathbf{x}) + \frac{Q_\eta \eta^2}{2} + \int_0^t \eta 3Nk_B T_0 \, \mathrm{d}t, \tag{52}$$

is a constant of motion for all t. While $\dot{E}_{NH} = 0$, the rate at which the energy of the system changes is given by:

$$\begin{aligned} E &= \sum \frac{p_i^2}{2m} + \Phi(\mathbf{x}) \Rightarrow \frac{\mathrm{d}E}{\mathrm{d}t} \\ &= -\sum \frac{\eta p_i^2}{m}. \end{aligned} \tag{53}$$

By definition, if no work is done on/by the system, it only exchanges heat energy with the thermostat. Consequently, applying the First Law of thermodynamics provides the rate of heat flow ($\dot{Q}$) in NH thermostatted dynamics: $\dot{E} = \dot{Q} \Rightarrow \dot{Q} = -\sum \eta p_i^2/m$. Under steady-state conditions: $\frac{\mathrm{d}}{\mathrm{d}t}\langle \frac{Q_\eta \eta^2}{2} \rangle = 0 \Rightarrow \langle \sum \eta p_i^2/m \rangle = 3N\langle \eta \rangle k_B T_0$, so that one can write:

$$\langle \dot{Q} \rangle = -\left\langle \sum \frac{\eta p_i^2}{m} \right\rangle = -3N\langle \eta \rangle k_B T_0 \tag{54}$$

This simple equation enables us to relate the dynamical heat flow characteristics with the phase-space properties. For example, in equilibrium, $\langle \dot{Q} \rangle = 0 \Rightarrow \langle \eta \rangle = 0$. However, instantaneously, $\dot{Q} \neq 0$ even in equilibrium (see fluctuation theorem [63]), which suggests that $\eta(t) \neq 0 \forall t$. As discussed previously, similar information is obtained by looking at Λ, the phase-space compression factor. The heat-flow entropy rate, defined as: $\langle \dot{S} \rangle = -\langle \dot{Q} \rangle / T_0$ signifies that in non-equilibrium $\langle \eta \rangle > 0$. Thus, while in equilibrium, the phase-space neither contracts nor expands in an averaged sense, the phase-space volume continuously shrinks and collapses to a dimension smaller than the embedding dimension in non-equilibrium cases.

Further, since the sum of the Lyapunov exponents, $\sum L_i$, provides the rate at which the phase-space volume changes, both $\langle \Lambda \rangle$ and $\langle \dot{S} \rangle$ are related to it:

$$\langle \Lambda \rangle = \sum_i L_i \Rightarrow \frac{\langle \dot{S} \rangle}{k_B} = -\sum_i L_i \tag{55}$$

For non-equilibrium problems, this equivalence occurs under the special condition that the temperature field, T_0, is constant. The equivalence is violated if the temperature field is position-dependent, such as the one shown in equation (13). The Gibbs' heat flow entropy, in this case, is given by:

$$\begin{aligned} \left\langle \frac{\dot{S}}{k_B} \right\rangle &= \left\langle \frac{-\dot{Q}}{k_B T} \right\rangle = \left\langle \frac{\sum \eta p_i^2}{mT} \right\rangle \\ &\neq \frac{\langle \sum \eta p_i^2/m \rangle}{\langle k_B T \rangle} = 3N\langle \eta \rangle = \langle -\Lambda \rangle \end{aligned} \tag{56}$$

However, a slight modification in the equations of motion (49) resolves the problem:

$$\begin{aligned} \frac{\mathrm{d}x_i}{\mathrm{d}t} &= \frac{p_i}{m}, \quad \frac{\mathrm{d}p_i}{\mathrm{d}t} = -\frac{\partial \Phi}{\partial x_i} - \eta p_i, \\ \frac{\mathrm{d}\eta}{\mathrm{d}t} &= \frac{1}{Q_\eta}\left[\frac{\sum p_i^2/m}{3Nk_B T} - 1 \right]. \end{aligned} \tag{57}$$

Imposing steady-state conditions,

$$\frac{\mathrm{d}}{\mathrm{d}t}\left(\frac{\langle Q_\eta \eta^2 \rangle}{2} \right) = 0 \Rightarrow \left\langle \frac{\sum \eta p_i^2/m}{k_B T} \right\rangle = \langle 3N\eta \rangle, \tag{58}$$

on the time-averaged rate of heat-flow entropy, we get

$$\left\langle \frac{\dot{S}}{k_B} \right\rangle = \left\langle \frac{\sum \eta p_i^2/m}{k_B T} \right\rangle = \langle 3N\eta \rangle = -\langle \Lambda \rangle. \tag{59}$$

The remarkable ability of the NH thermostat to link the dynamical variables with their thermodynamic counterparts has made it very popular amongst researchers. The NH thermostat performs well for large equilibrium as well as non-equilibrium problems, having been verified experimentally as well [64].

The NH thermostat has spurred the development of several thermostat algorithms, each with its own merit. Watanabe and Kobayashi [18] relaxed the assumption of $\partial\dot{\eta}/\partial\eta = 0$, and generalised the Nosé-Hoover equations. Working with Jellinek and Berry's generalisation of Nosé Hamiltonian [57], which results in a more efficient mixing of phase-space trajectories, Brańka and Wojciechowskie generalised the Nosé-Hoover dynamics [65] to obtain improved thermalising characteristics in an SHO. Using the Guessing Method, Bravetti and Tapias [66] developed equations of motion that generate any target density distribution.

For a large system, one can use Gear's predictor-corrector method [67] for solving the NH equations of motion (49). In here, the variables are first predicted based on a Taylor's series expansion, and then corrected with respect to a higher-order derivative of acceleration. However, the time-reversibility of the equations of motion is lost along with the symplectic property of the dynamics. While for a small system, the 4^{th} order Runge-Kutta method may be used, the method is time-consuming, not symplectic, and causes a long-term energy drift. Martyna and coworkers [68] have developed a symplectic algorithm based on Trotter's factorisation and Liouville's operators, which may be used for a large system.

The NH thermostat satisfies almost all qualities of a 'good' thermostat – (i) it is time-reversible: if we reverse each momentum term such that $p_i \to -p_i$ and $\eta \to -\eta$, the path is traced back, (ii) it conforms with the laws of thermodynamics and allows heat to flow from a hotter thermostat to a colder thermostat, and (iii) it is easy to implement. But, the dynamics is not ergodic [17], as we shall see later. In general, it is thought that the issue of non-ergodicity of the NH thermostat can be tackled by using multi-variable thermostats [12,18,50,52,69]. We now describe these multi-variable thermostats.

4.2.3. Martyna-Klein-Tuckerman thermostat

One of the major breakthroughs in improving the ergodic characteristics of a single-particle system thermostatted using

the NH thermostat was the development of the Nosé-Hoover chain (MKT) thermostat [50,51]. In this approach, the kinetic temperature of the system is controlled along with the fluctuations of the heat-bath variable through additional variables. Simply put, while the thermostat variable η_1 controls the kinetic temperature of the system similar to that in the NH thermostat, the fluctuations of η_1 are controlled by another variable η_2. Likewise, the fluctuations of η_2 are controlled by a third thermostat variable, η_3, and so on. Thus, a chain of thermostats (η_1, η_2, …, η_k) is formed. The MKT equations of motion are:

$$\begin{aligned}
\dot{x}_i &= \frac{p_i}{m},\\
\dot{p}_i &= \frac{\partial \Phi}{\partial x_i} - p_i \frac{\eta_1}{Q_{\eta_1}},\\
\dot{\eta}_1 &= \left[\sum_{i=1}^{3N} \frac{p_i^2}{m_i} - 3Nk_BT_0\right] - \eta_1 \frac{\eta_2}{Q_{\eta_2}},\\
&\vdots\\
\dot{\eta}_j &= \left[\frac{\eta_{j-1}^2}{Q_{\eta_{j-1}}} - k_BT_0\right] - \eta_j \frac{\eta_{j+1}}{Q_{\eta_{j+1}}}\\
&\vdots\\
\dot{\eta}_k &= \left[\frac{\eta_{k-1}^2}{Q_{\eta_{k-1}}} - k_BT_0\right].
\end{aligned} \tag{60}$$

The variable Q_{η_i} may be thought of as the mass associated with the heat-bath variable η_i. An empirical rule of selecting the thermostat masses is: $Q_{\eta_1} = 3Nk_BT_0/\omega^2$ and $Q_{\eta_{j\neq 1}} = k_BT_0/\omega^2$ [50,51]. The frequency, ω, describes the frequency with which the kinetic energy oscillates between the system and the reservoirs. A lot of approximations have gone in developing this relationship, and a suitable choice is usually problem-dependent. We will see later how the dynamics changes substantially depending on the choice of Q_{η_i}, especially for small-scale systems.

Due to the presence of k heat-bath variables, the extended phase space is $6N+k$ dimensional: $\mathbf{\Gamma} = (\mathbf{x}, \mathbf{p}, \eta_1, \eta_2, \ldots, \eta_k)$. The MKT equations satisfy the steady-state Liouville's Equation (38) with the extended phase-space distribution as:

$$f_{\text{ex}}(\mathbf{\Gamma}) \propto \exp\left[-\beta_0\left(H + \sum_{i=1}^{k} \frac{\eta_i^2}{2Q_{\eta_i}}\right)\right]. \tag{61}$$

Here, $H = \sum p_i^2/2m + \Phi(\mathbf{x})$. The pseudo energy for the MKT equations of motion, which is a constant of motion, is given by:

$$\begin{aligned}
E_{\text{MKT}} = &\left(H + \sum_{i=1}^{k} \frac{\eta_i^2}{2Q_{\eta_i}}\right)\\
&+ k_BT_0 \int_0^t \left[3N\frac{\eta_1}{Q_{\eta_1}} + \sum_{2}^{k} \frac{\eta_i}{Q_{\eta_i}}\right] \mathrm{d}t.
\end{aligned} \tag{62}$$

Like the NH thermostat, the dynamical variables of an MKT thermostatted system may be linked with the thermodynamic quantities:

$$\begin{aligned}
\dot{E} = \dot{Q} &= \sum_{i=1}^{3N}\left(\frac{\partial \Phi}{\partial x_i}\dot{x}_i + \frac{p_i}{m}\dot{p}_i\right) = \sum_{i=1}^{3N} \frac{-\eta_1 p_i^2}{mQ_{\eta_1}},\\
\dot{S} &= -\frac{\dot{Q}}{T_0} = \frac{-\eta_1}{mQ_{\eta_1}} \sum_{i=1}^{3N} \frac{p_i^2}{T_0},\\
\Lambda &= -3N\frac{\eta_1}{Q_{\eta_1}} - \sum_{i=2}^{k} \frac{\eta_i}{Q_{\eta_i}}
\end{aligned} \tag{63}$$

Recalling that in steady-state:

$$\left\langle \frac{\mathrm{d}}{\mathrm{d}t}\left(\sum_{i=1^k} \frac{\eta_i^2}{2Q_{\eta_1}}\right)\right\rangle = 0, \tag{64}$$

$\langle \dot{Q} \rangle$ and $\langle \dot{S} \rangle$ may be written as:

$$\begin{aligned}
\langle \dot{Q} \rangle &= -k_BT_0\left[3N\frac{\langle \eta_1 \rangle}{Q_{\eta_1}} + \sum_{2}^{k} \frac{\langle \eta_i \rangle}{Q_{\eta_i}}\right],\\
\left\langle \frac{\dot{S}}{k_B} \right\rangle &= -\left\langle \frac{\dot{Q}}{k_BT_0} \right\rangle = \left[3N\frac{\langle \eta_1 \rangle}{Q_{\eta_1}} + \sum_{2}^{k} \frac{\langle \eta_i \rangle}{Q_{\eta_i}}\right] = -\langle \Lambda \rangle
\end{aligned} \tag{65}$$

Note that like the NH thermostat, the formulation of the MKT thermostat shown in Equation (60) satisfies Equations (65) in equilibrium and non-equilibrium states where the desired temperature T_0 does not change. In cases where T_0 is position-dependent, the MKT equations require a modification similar to that shown in Equation (57). Again, like the NH thermostat, $\langle \Lambda \rangle$ is zero in equilibrium and non-zero in non-equilibrium. In both the situations, $\langle \Lambda \rangle$ can be related to $\sum L_i$. However, unlike the NH thermostat, the MKT thermostat does not have any known Hamiltonian from which the equations of motion can be derived.

The most popular variant of the MKT thermostat is the two-chain variant, for which the equations of motion are:

$$\begin{aligned}
\dot{x}_i &= \frac{p_i}{m},\\
\dot{p}_i &= \frac{\partial \Phi}{\partial q_i} - p_i \frac{\eta}{Q_\eta},\\
\dot{\eta} &= \left[\sum_{i=1}^{3N} \frac{p_i^2}{m_i} - 3Nk_BT_0\right] - \frac{\eta\xi}{Q_\xi},\\
\dot{\xi} &= \left[\frac{\eta^2}{Q_\eta} - k_BT_0\right].
\end{aligned} \tag{66}$$

These equations of motion may be solved using the Runge-Kutta technique for small-scale systems like a harmonic oscillator. However, for large systems, the symplectic technique, based on Lie-Trotter factorisation and Liouville's operators, developed by Martyna and coworkers [68] is more suitable.

We will explore the ergodic and the dynamical characteristics of the MKT thermostat later in this review.

4.2.4. Hoover-Holian thermostat

The two-variable Hoover-Holian (HH) thermostat takes a different approach than the MKT thermostat to improve the

ergodic characteristics. It is based on the kinetic-moments method [52], wherein the first two moments of the kinetic energy (see Equation (18)) are controlled to remove the errors associated with them. Each moment is controlled through a different heat-bath variable, and hence the extended phase-space, $\mathbf{\Gamma} = (\mathbf{x}, \mathbf{p}, \eta, \xi)$, comprises $6N+2$ dimensions. Note that for a system to follow the 'true' Maxwell-Boltzmann distribution, errors associated with *all* moments must be removed. However, doing so would result in very stiff differential equations. If the dynamics is ergodic, it is expected that given sufficient time, the dynamics is sampled in a manner that errors associated with the higher-order moments get removed as well.

The HH thermostat may be developed using a modified form of the guessing method. We begin with the coupling:

$$\dot{x}_i = p_i,\ \dot{p}_i = F_i - \eta p_i - \xi(K/K_0)p_i. \tag{67}$$

Here, $K_0 = (3N/2)k_BT_0$, is the desired kinetic energy, and K, the instantaneous kinetic energy. Solving the steady-state Liouville's equation with the extended phase-space distribution,

$$f_{\text{ex}}(\mathbf{\Gamma}) \propto \exp\left(-\beta\left[H + K_0 Q_\eta \eta^2 + K_0 Q_\xi \xi^2\right]\right), \tag{68}$$

gives the equation of motion:

$$\begin{aligned}
\dot{x}_i &= p_i \\
\dot{p}_i &= F_i - \eta p_i - \xi\left(\frac{K}{K_0}\right)p_i \\
\dot{\eta} &= \frac{1}{Q_\eta}\left[\frac{K}{K_0} - 1\right] \\
\dot{\xi} &= \frac{1}{Q_\xi}\frac{K}{K_0}\left[\frac{K}{K_0} - 1 - \frac{2}{3N}\right]
\end{aligned} \tag{69}$$

The coupling shown in Equation (67) may be viewed as two independent thermal reservoirs simultaneously acting on the system – one for controlling the first moment of kinetic energy (η) and the other for controlling the second moment (ξ). These equations are applicable to equilibrium and nonequilibrium many-body simulations. They are time-reversible, ergodic, conform with the different laws of thermodynamics and easy to implement. However, a Hamiltonian basis for these equations of motion is yet to be discovered, even though a constant of motion exists:

$$\begin{aligned}
E_{\text{HH}} = \Phi(\mathbf{x}) + \sum_{i=1}^{3N}\frac{p_i^2}{2m} + K_0\left(Q_\eta\eta^2 + Q_\xi\xi^2\right) \\
+ \int_0^t\left[2K_0\eta + K\xi\left(1 + \frac{2}{3N}\right)\right]\mathrm{d}t
\end{aligned} \tag{70}$$

In comparison to the MKT thermostat, the equations of motion are stiffer as they involve a term containing K^2. Consequently, a smaller time-step may be required to solve them accurately. These equations can be readily modified to incorporate higher order moments of kinetic energy, but the resulting differential equations become very stiff (since they have K^3 or higher-order terms), necessitating small integration time-steps and increasing the computational cost. Just like in the MKT thermostat, where additional thermostat variables are introduced to control the fluctuations of thermostat variables, the Hoover-Holian thermostat can be generalised to include additional thermostat variables to control the fluctuations of η and ξ [70].

A closely related approach to the HH thermostat is the algorithm that controls the first two even moments of velocity, for which the temperatures being controlled are as per Equations (14) and (18). When this thermostat is coupled with an SHO, the resulting equations of motion are identical to that shown in Equations (101), and consequently all thermodynamic properties are identical. However, for a multi-particle system, the equations of motion for the two thermostats are different.

The ergodic characteristics of the HH thermostat along with its response in different non-equilibrium problems are discussed later in this review.

4.2.5. Campisi-Zhan-Talkner-Hangii thermostat

All extended-system based thermostats described so far represent further developments of the Nosé thermostat. Campisi et al. [53,54] recently proposed a new Hamiltonian based thermostat that possesses infinite heat capacity, and does not involve time-scaling variables. This thermostat, also known as the log thermostat, comprises an oscillator of mass m_s governed by the Hamiltonian:

$$H_{\text{CZTH}} = \frac{p_s^2}{2m_s} + \frac{k_BT_0}{2}\log\left(s^2 + \delta\right), \tag{71}$$

where, s and p_s denote the position and momentum of the oscillator, respectively. In order to prevent singularity of the potential energy at the origin, a small constant δ is usually added. The kinetic temperature of the oscillator is independent of the total energy of the oscillator, and is always equal to k_BT_0. This can be easily proved by employing the Virial theorem under the assumption that $\delta \ll 1$:

$$\left\langle p_s\frac{\partial H_{\text{CZTH}}}{\partial p_s}\right\rangle = \left\langle s\frac{\partial H_{\text{CZTH}}}{\partial s}\right\rangle \Rightarrow \left\langle\frac{p_s^2}{m}\right\rangle = k_BT_0. \tag{72}$$

Further, the momentum-space sampled by the dynamics is according to the Maxwell-Boltzmann distribution. Being Hamiltonian, the dynamics is time-reversible as well. So, the log thermostat satisfies several properties of a good thermostat – it's time reversible, possesses a Hamiltonian and samples the phase-space according to the Maxwell-Boltzmann distribution.

Let the physical system to be thermostatted comprise N particles and possess an Hamiltonian $H = \sum p_i^2/2m + \Phi(\mathbf{x})$. When coupled to the log thermostat through a coupling function $h(\mathbf{x}, s)$, an extended system comprising the physical system and the log thermostat is obtained. The extended system is, therefore, governed by the Hamiltonian:

$$H_{\text{ex}} = H_{\text{CZTH}} + H(\mathbf{x}, \mathbf{p}) + h(\mathbf{x}, s). \tag{73}$$

The coupling function, $h(\mathbf{x}, s)$, ensures the interaction between the system and the log thermostat. In its absence, the system and the log thermostat undergo microcanonical dynamics independently. Ideally, $h(\mathbf{x}, s)$ should be chosen such that

ergodicity is imparted within the system. However, the selection of appropriate coupling functions remains a problem open to research. The equations of motion obtained from H_{ex} are:

$$\begin{aligned} \dot{x}_i &= \frac{p_i}{m}, \quad \dot{p}_i = -\frac{\partial \Phi}{\partial x_i} - \frac{\partial h(\mathbf{x}, s)}{\partial x_i}, \\ \dot{s} &= p_s, \quad \dot{p}_s = \frac{k_B T_0 s}{s^2+\delta} - \frac{\partial h(x, s)}{\partial x}. \end{aligned} \tag{74}$$

These equations can be integrated using the Velocity-Verlet algorithm (see Equation (3)). Note that the presence of δ, which was added to H_{CZTH} to prevent any singularity as $s \to 0$, causes deviation of the momentum distribution from the Maxwell-Boltzmann distribution [54]. The deviation is more pronounced as N increases. This limits the usefulness of log thermostat to systems comprising very few particles.

Despite the theoretical advantages of the log thermostat, several problems emerge when one tries to employ it in standard MD simulations:

(1) The log thermostat does not conform with the Zeroth Law of thermodynamics [71]. When an SHO, in thermal equilibrium at T_0, is coupled using harmonic springs with two log thermostats, also kept at T_0, the temperature of the log thermostats no longer remains at T_0, which is a clear violation of the Zeroth Law of thermodynamics. Such a problem is not observed in other thermostats.
(2) The log thermostat fails to promote heat flow [72]. When a one-dimensional Φ^4 chain is coupled to two log thermostats kept at different temperatures, no heat flow occurs, which is a clear violation of the Second Law of thermodynamics.
(3) The configurational temperature associated with the log thermostat is negative in one dimension and zero in two dimension [73], which is an unphysical situation.
(4) The log thermostat violates the equipartition theorem along with the virial theorem for strong coupling to the system. [74].

Because of these problems, the thermostat has not gained wide acceptability in the MD community. We will explore some of these issues towards the later part of this review.

5. Rugh's temperature and its control

So far, we have discussed kinetic temperature and its control. The kinetic temperature relates β with *only* the momentum variables. A careful look at the Maxwell-Boltzmann distribution, shown in Equation (16) suggests that β is associated with both momentum and configurational variables. So, intuitively one may expect β to be related to all the phase-space variables. Rugh's temperature precisely does this – in Rugh's approach, the temperature is determined from the global geometric structure of the total energy surface [75,76]. It was later observed that the Rugh's temperature is a particular case of a more generalised situation: consider a continuous differentiable phase functional, B, the temperature of a system in equilibrium is related to it through [77]:

$$\frac{1}{k_B T} = \left\langle \frac{\nabla.\nabla B}{\nabla B.\nabla H} \right\rangle \equiv \frac{\langle \nabla.\nabla B \rangle}{\langle \nabla B.\nabla H \rangle}. \tag{75}$$

Here, ∇ is the gradient with respect to both configurational and momentum variables. This expression of temperature is independent of the choice of ensemble, and is equally applicable to microcanonical, canonical and MD ensembles [77].

Under very general conditions, it has been shown that, in equilibrium, the choice of B does not influence the numerical value of the temperature. It is, therefore, possible to obtain a family of temperature definitions by choosing an appropriate functional form of B. For example, the different measures of kinetic temperature can be obtained from Equation (75): the usual kinetic temperature (Equation (14)) is obtained by choosing $B = \sum p_i^2/2$, while choosing $B = \sum p_i^4/4$ leads to $T_{k,2}$. Likewise, one can obtain $T_{K,2}$ by choosing $B = K^2$.

The Rugh's temperature, T_R, is obtained by choosing $B = H = K + \Phi$ in (75):

$$\frac{1}{k_B T_R} = \frac{\langle \nabla^2 K + \nabla^2 \Phi \rangle}{\langle (\nabla K)^2 + (\nabla \Phi)^2 \rangle}. \tag{76}$$

Apart from taking into account the momentum variables through the terms ∇K and $\nabla^2 K$, T_R, separately considers the configurational variables through the terms $\nabla\Phi$ and $\nabla^2\Phi$. A closer look at Equation (76) reveals a dimensional inconsistency that can be corrected by multiplying a unit constant of appropriate dimensions to both numerator and denominator [78]. Extension of equilibrium Rugh's temperature to nonequilibrium cases also exists [78].

The need to control T_R arises from the requirement of correctly simulating the near-equilibrium problems, where the local thermodynamic equilibrium (LTE) hypothesis holds. Under LTE conditions, all postulates of equilibrium thermodynamics are applicable *locally*, including: (i) the agreement of the local velocity distribution with the Maxwell-Boltzmann distribution, and (ii) the numerical agreement locally between the different ways of defining the temperature. In near-equilibrium problems simulated using the kinetic thermostats, although the velocity distribution agrees with the Maxwell-Boltzmann distribution locally, there is a significant difference between T_k and T_R [72,79,80]. MD simulations of isothermal Couette flow reveal that a heat flow occurs even in the absence of any temperature gradient when the kinetic thermostats are used [81]. To accurately account for the heat flow, one needs to bring in Rugh's temperature [82]. Further, the dynamical properties of a microscopic system subjected to near-equilibrium conditions depend on the definition of temperature being controlled [83,84].

As of now, only two approaches are available for controlling T_R – the Patra-Bhattacharya thermostat and the Bauer-Bulgac-Kusnezov thermostat, both based on the extended-system method described previously. Let us briefly describe these algorithms.

5.1. Patra-Bhattacharya thermostat

The Patra-Bhattacharya (PB) thermostat uses two thermostat variables – η and ξ – for separately controlling both momentum and configurational variables such that T_R gets controlled. Choosing $h_1(\xi) = \xi$, $C_i(x_i, p_i) = \frac{\partial \Phi}{\partial x_i}$, $h_2(\eta) = \eta$ and $D_i(x_i, p_i) = p_i$ in Equation (37) provides the equation of

motion of the PB thermostat:

$$\begin{aligned}\dot{x}_i &= \frac{p_i}{m} - \xi\frac{\partial\Phi}{\partial x_i},\\ \dot{p}_i &= -\frac{\partial\Phi}{\partial x_i} - \eta p_i,\\ \dot{\xi} &= \frac{1}{Q_\xi}\sum_{i=1}^{3N}\left[\left(\frac{\partial\Phi}{\partial x_i}\right)^2 - k_B T_0\frac{\partial^2\Phi}{\partial x_i^2}\right],\\ \dot{\eta} &= \frac{1}{Q_\eta}\sum_{i=1}^{3N}\left[\frac{p_i^2}{m} - k_B T_0\right].\end{aligned} \tag{77}$$

The extended phase-space distribution corresponding to the PB thermostat is given by:

$$f_{\text{ex}}(\mathbf{\Gamma}) \propto \exp\left(-\beta\left[H + \frac{Q_\eta\eta^2}{2} + \frac{Q_\xi\xi^2}{2}\right]\right). \tag{78}$$

Like other extended-system based thermostats, the rate at which a system approaches a canonical ensemble is dependent on Q_η and Q_ξ [51,85]. The fluctuation of T_R is significantly influenced by these parameters. It is important to note that for a large-system, $Q_\eta \neq Q_\xi$, since the changes in the configurational variables occur over a longer time-scale than the momentum variables. So depending on the problem being simulated, Q_ξ can be one (or more) order of magnitude different from Q_η. Similar to the HH and the MKT thermostats, the PB thermostat does not possess a Hamiltonian, but a pseudo-energy, which is a constant of motion, exists:

$$\begin{aligned}E_{\text{PB}} = \Phi(\mathbf{x}) &+ \sum_{i=1}^{3N}\frac{p_i^2}{2m} + \frac{Q_\eta\eta^2}{2} + \frac{Q_\xi\xi^2}{2}\\ &+ k_B T_0\int_0^t\left(3N\eta + \sum_{i=1}^{3N}\frac{\partial^2\Phi}{\partial x_i^2}\right)\mathrm{d}t\end{aligned} \tag{79}$$

While the equations of motion (77) do not result in: $\langle\dot{S}\rangle/k_B = \langle\Lambda\rangle$ for non-equlibrium cases with position-dependent T, modifications performed similar to the NH thermostat can resolve the issue. Apart from giving more consistent results in non-equilibrium thermal conduction, the Patra-Bhattacharya thermostat can be utilised for creating a thermal gradient between the configurational and the kinetic degrees of freedom. Such unique thermostatting capability provides an ability to engineer thermal rectification [86].

The PB thermostat satisfies several properties of a good thermostat – it is time-reversible, conforms to the different laws of thermodynamics, including the spontaneous flow of heat between a hotter and a colder thermostat, and is simple to implement for systems with pair-wise interacting particles. However, the dynamics of a single-particle system coupled to this thermostat is non-ergodic, the details of which will be seen later in this review. Further, for systems with multi-body interactions or where the analytical form of interaction potential is not readily available, the PB thermostat is computationally more expensive than the kinetic temperature based thermostats. This is because of the need to numerically compute the diagonal elements of the Hessian matrix, $\nabla^2\Phi$, which requires $O(N^3)$ operations. As of now, symplectic algorithms for integrating the PB equations are not available. The equations may be integrated using Gear's predictor-corrector algorithm [87].

5.2. Bauer-Bulgac-Kusnezov thermostat

The Bauer-Bulgac-Kusnezov (BBK) thermostat traces its origin to the early 1990s, before the concept of Rugh's temperature arose. The objective of Bauer and coworkers was to clarify and generalise the origins of the NH thermostat [16,55]. They sought a better coupling than the NH method for improving its ergodic characteristics. As it turns out, their approach can be used for controlling Rugh's temperature as well. The basic equations of the BBK thermostat are discussed before (see Equations (37) and (40)), and hence, not described in details in this section.

The BBK thermostat shows that the dynamics is sampled from a canonical ensemble by controlling the ratio of two quantities: $\frac{\partial C_i/\partial x_i}{C_i.\partial\Phi/\partial x_i}$ and $\frac{\partial D_i/\partial p_i}{D_i.\partial\Phi/\partial p_i}$. For example,

$$\begin{aligned}k_B T_0\left\langle\frac{\partial D_i}{\partial p_i}\right\rangle &= \frac{1}{Z}k_B T_0\int\frac{\partial D_i}{\partial p_i}\exp\left(-\beta H\right)\mathrm{d}x\,\mathrm{d}p\\ &= -\frac{1}{Z}k_B T_0\int D_i.\frac{\partial}{\partial p_i}\exp\left(-\beta H\right)\mathrm{d}x\,\mathrm{d}p\\ &= \left\langle D_i.\frac{\partial\Phi}{\partial p_i}\right\rangle.\end{aligned} \tag{80}$$

The Rugh's temperature may be controlled with the following choice of the variables C and D:

$$C(x_i, p_i) = \frac{\partial\Phi}{\partial x_i} \quad \text{and} \quad D(x_i, p_i) = p_i \tag{81}$$

The benefit of this thermostat is that it enables the choice of coupling functions that enhance phase-space mixing characteristics, and consequently, have improved ergodic properties over the PB thermostat. For example, with a cubic coupling the equations of motion become:

$$\begin{aligned}\dot{x}_i &= \frac{p_i}{m} - \xi^3\frac{\partial\Phi}{\partial x_i},\\ \dot{p}_i &= -\frac{\partial\Phi}{\partial x_i} - \eta^3 p_i,\\ \dot{\xi} &= \frac{1}{Q_\xi}\sum_{i=1}^{3N}\left[\left(\frac{\partial\Phi}{\partial x_i}\right)^2 - k_B T_0\frac{\partial^2\Phi}{\partial x_i^2}\right],\\ \dot{\eta} &= \frac{1}{Q_\eta}\sum_{i=1}^{3N}\left[\frac{p_i^2}{m} - k_B T_0\right].\end{aligned} \tag{82}$$

The Bauer-Bulgac-Kusnezov thermostat permits coupling of any arbitrarily higher order, but that comes at a price – the equations of motion become stiff. They require very small time steps for an accurate solution. Overall, this thermostat has only been used for pedagogical purposes, despite it being time-reversible and showing improved ergodic characteristics. Being a part of the Nosé-Hoover family, it satisfies the different laws of thermodynamics, and is able to show heat flow from a hotter thermostat to a colder thermostat spontaneously.

6. Configurational temperature and its control

The generalised temperature-curvature relationship, shown in Equation (75), opened up the possibility of defining the temperature of a microscopic system solely in terms of the configurational variables. If B in Equation (75) is chosen such that it is a scalar functional of only the particles' coordinates and not momenta, the temperature of the system depends only on the microscopic configuration of the particles. Hence, this temperature is called the configurational temperature. Perhaps, the most common way of defining configurational temperature, T_C, is obtained by choosing $B = \Phi(\mathbf{x})$ [77,88,89]:

$$\frac{1}{k_B T_C} = \frac{\langle \nabla^2 \Phi \rangle}{\langle (\nabla \Phi)^2 \rangle}, \tag{83}$$

Remarkably, the same expression appears almost half a century ago in Landau and Lifshitz' textbook on statistical physics [90], where it is shown that T_C can be obtained through a single integration by parts of the expression:

$$\langle \nabla_x^2 H \rangle_C = \frac{\langle (\nabla_x H)^2 \rangle_C}{k_B T_C}, \tag{84}$$

where, $\langle \ldots \rangle_C$ denotes the averaging performed with respect to the canonical distribution.

Other common ways of defining the configurational temperature draw inspiration from higher order measures of the kinetic temperature. If we take $B = \Phi^2$ in the generalised temperature-curvature relationship we obtain the second order configurational temperature:

$$\frac{1}{k_B T_{C,2}} = \frac{\langle \Phi \nabla^2 \Phi + \| (\nabla \Phi)^2 \| \rangle}{\langle \Phi \| (\nabla \Phi)^2 \| \rangle}, \tag{85}$$

Likewise, one can obtain even higher order measures of configurational temperature.

Computation of the configurational temperature and its control are necessary for situations where controlling the kinetic temperature, T_k, results in spurious results, such as, non-equilibrium problems of shockwave propagation, non-equilibrium MD simulations of certain heat-driven processes [40,91] and flowing systems with spatial and possibly time-varying streaming velocity. During shockwave propagation, the kinetic temperature in one direction is significantly higher than the rest two [92,93], and consequently, thermostatting the entire simulation domain at a fixed kinetic temperature may not be correct. The breakdown of the equipartition theorem here renders T_k to behave as a tensorial quantity which is difficult to reconcile with the thermodynamic definition of temperature. Controlling T_C is superior in this situation as the equipartition theorem is not necessary to define T_C. Using T_C over T_k is advantageous in another class of non-equilibrium problems – shear flow. Here, the streaming velocity must be known beforehand for calculating the peculiar kinetic energy, which serves as an input to T_k. The inability of correctly determining the streaming velocity leads to several problems like stabilisation of string phases [40,91,94], creation of anti-symmetric stress components [95], etc. Using T_C is also advantageous in thermostatting biological molecules, which are usually geometrically constrained, and more often than not, comprise several non-translational degrees of freedom, like planar rotation, bond rotation, etc. In such cases, thermostatting the three translation degrees of freedom, as is done for T_k, may not be sufficient [96]. While in equilibrium, controlling any one kind of temperature necessary implies an automatic control of all other measures of temperature, in non-equilibrium, there is no theory which suggests that the different measures of temperature should agree with each other. In fact, in strongly non-equilibrium problems, $T_k \neq T_R \neq T_C$, and it is not known which of the three gives a closer approximation to the 'reality'.

Note that calculating T_C is challenging in systems where the particles are non-interacting or interact negligibly, such as in perfect gases. In these cases, both the numerator, $\langle (\nabla \Phi)^2 \rangle$) and the denominator, $\langle \nabla^2 \Phi \rangle$, of $T_C \to 0$, making T_C indeterminate. The Rugh's temperature, T_R, as well the kinetic temperature, T_k, in the limit of perfect gases, are finite, though. For systems interacting with complex interatomic potentials, the computation of T_C requires numerically calculating the Hessian matrix, which is computationally expensive.

The first configurational thermostat was developed on the lines of the GIK thermostat by Delhommelle and Evans [44,97]. Gauss' principle of least constraint was used with the holonomic constraint (without the average) shown in equation (83). However, the utility of this thermostat is found to be low since the equations of motion contain terms involving the third-order gradient of $\Phi(\mathbf{x})$. The equations of motion are stiff as well. In a bid to alleviate these problems, a separate configurational thermostat was created for thermostatting the *slow configurational* variables selectively [98] through the Smoluchowski equation. Under the assumption that the momentum variables relax much faster than the configurational variables, the momentum evolution equations were completely dropped.

We will now discuss the development of the Braga-Travis thermostat, the C_{12} thermostat and the virial thermostat, which are based on the extended system method.

6.1. Braga-Travis (BT) thermostat

Braga and Travis [96,99,100] adopted the route of the NH thermostat for controlling the configurational temperature. Based on the extended system method, the BT thermostat uses an additional reservoir variable so that the extended phase-space comprises $6N+1$ degrees of freedom. Choosing $h_1(\xi) = \xi$, $C_i(x_i, p_i) = \frac{\partial \Phi}{\partial x_i}$, $h_2(\eta) = 0$ and $D_i(x_i, p_i) = 0$ in Equation (37) provides the equation of motion of the BT thermostat:

$$\begin{aligned} \dot{x}_i &= \frac{p_i}{m_i} - \xi \frac{\partial \Phi}{\partial x_i}, \\ \dot{p}_i &= -\frac{\partial \Phi}{\partial x_i} \\ \dot{\xi} &= \frac{1}{Q_\xi} \sum_{i=1}^{3N} \left[\left(\frac{\partial \Phi}{\partial x_i} \right)^2 - k_B T_0 \frac{\partial^2 \Phi}{\partial x_i^2} \right]. \end{aligned} \tag{86}$$

In equilibrium, where $\langle \xi \rangle = 0$, $\langle \dot{\xi} \rangle$ must also equal zero, from which it is trivial to show that the desired temperature, T_0, equals

the configurational temperature T_C. The extended phase-space distribution function satisfied by the BT equations of motion is given by:

$$f_{\text{ex}}(\mathbf{\Gamma}) \propto \exp\left(-\beta\left[H + \frac{Q_\xi \xi^2}{2}\right]\right). \tag{87}$$

The BT equations of motion are time-reversible, easy to implement for microscopic systems with pair-wise interaction potential and satisfy the Zeroth Law and the Second Law of thermodynamics. These equations, however, do not have any Hamiltonian associated with them, and like the NH thermostat, result in non-ergodic dynamics for a single-particle system. The BT thermostat is gaining popularity for simulating non-equilibrium problems described before.

The BT thermostat has seen many improvements over the years, and now, several variants exist, such as, the thermostat which includes bond-length constraints [100] suited for long-chain molecules, a stochastic analog [101], and the Braga-Travis chain thermostat which is the configurational counterpart of the Nosé-Hoover chain thermostat [102].

6.2. $C_{1,2}$ thermostat

The $C_{1,2}$ thermostat was proposed to improve the ergodic characteristics of the BT thermostat [103]. It is an extension of the BT thermostat for simultaneously controlling the first two orders of configurational temperature. This is achieved by introducing two heat-bath variables. The algorithm is similar to the HH thermostat, where two thermostat variables are employed for controlling the first two moments of kinetic energy. Controlling the second-order configurational temperature, $T_{C,2}$, shown in Equation (85), along with the first order configurational temperature, T_C, shown in Equation (83) removes the errors associated with the incorrect sampling of the phase-space especially in very small-scale systems.

The equations of motion are given by:

$$\begin{aligned}
\dot{x}_i &= \frac{p_i}{m_i} - \xi\frac{\partial\Phi}{\partial x_i} - 2\eta\Phi\frac{\partial\Phi}{\partial x_i},\\
\dot{p}_i &= -\frac{\partial\Phi}{\partial x_i},\\
\dot{\xi} &= \frac{1}{Q_\xi}\sum_{i=1}^{3N}\left[\left(\frac{\partial\Phi}{\partial x_i}\right)^2 - k_B T_0\frac{\partial^2\Phi}{\partial x_i^2}\right],\\
\dot{\eta} &= \frac{1}{Q_\eta}\sum_{i=1}^{3N}\left[\Phi\left(\frac{\partial\Phi}{\partial x_i}\right)^2 - k_B T_0\left(\Phi\frac{\partial^2\Phi}{\partial x_i^2} + \left(\frac{\partial\Phi}{\partial x_i}\right)^2\right)\right],
\end{aligned} \tag{88}$$

and the corresponding extended phase-space distribution is:

$$f_{\text{ex}}(\mathbf{x}, \mathbf{p}, \eta, \xi) \propto e^{-\beta\left[H + \frac{Q_\eta\eta^2}{2} + \frac{Q_\xi\xi^2}{2}\right]}. \tag{89}$$

Like the BT thermostat, the C_{12} equations of motion do not have a Hamiltonian basis, however, the following function:

$$\begin{aligned}
E_{C_{12}} = \Phi(\mathbf{x}) &+ \sum_{i=1}^{3N}\frac{p_i^2}{2m} + Q_\xi\frac{\xi^2}{2} + Q_\eta\frac{\eta^2}{2}\\
&+ \sum_{i=1}^{3N}\left[\eta(\Phi + k_B T_0)\left(\frac{\partial\Phi}{\partial x_i}\right)^2 + \xi k_B T_0\frac{\partial^2\Phi}{\partial x_i^2}\right.\\
&\left. + \eta k_B T_0\left(\Phi + \frac{\partial^2\Phi}{\partial x_i^2}\right)\right],
\end{aligned} \tag{90}$$

is a constant of motion.

While the C_{12} thermostat improves upon the ergodic properties vis-á-vis the BT thermostat, its numerical implementation also requires the computation of the diagonal elements of the Hessian matrix, a computationally expensive task. The C_{12} thermostat can be extended for controlling the first three orders of configurational temperature, however, the resulting equations of motion become stiffer. Overall, this thermostat has mostly been used for pedagogical purposes and has seen limited use in large-scale systems.

6.3. Virial thermostat

Long before the development of the generalised temperature-curvature relation, the virial theorem provided the only means for relating the kinetic energy of a system with its configurational variables. The virial theorem has been proved both in the framework of the classical thermodynamics and statistical mechanics [90]. Its validity does not require ergodicity of the underlying dynamics, so long as the kinetic energy is not related to the temperature. Mathematically, the theorem can be expressed as:

$$\left\langle\sum x_i\frac{\partial\Phi}{\partial x_i}\right\rangle_t = \left\langle\sum\frac{p_i^2}{m}\right\rangle_t \tag{91}$$

where, $\langle\ldots\rangle_t$ denotes time average. Note that the expression (91) remains valid in equilibrium as well as in non-equilibrium steady states. If one now brings the equipartition theorem, the expression may be rewritten as:

$$\left\langle\sum x_i\frac{\partial\Phi}{\partial x_i}\right\rangle = 3Nk_B T \tag{92}$$

The same expression for the temperature may be obtained from the generalised temperature-curvature relationship, (75), with $B = \sum x_i^2/2$. A careful look at Equation (92) shows that the mathematical expression of temperature is devoid of any momentum terms and involves only the configurational variables. In other words, the virial temperature may be treated as a special case of the configurational temperature.

The first attempt of controlling the Virial temperature began in the early 1990s. Hamilton and coworkers [104,105] developed the extended-system based equations of motion:

$$\begin{aligned}
\dot{x}_i &= \frac{p_i}{m} - \eta x_i, \qquad \dot{p}_i = -\frac{\partial\Phi}{\partial x_i},\\
\dot{\eta} &= \frac{1}{Q_\eta}\left[\sum x_i\frac{\partial\Phi}{\partial x_i} - 3Nk_B T_0\right],
\end{aligned} \tag{93}$$

to control the virial temperature. These equations of motion satisfy the generalised BBK Equations (37) and (40). It is interesting to note that these equations of motion have a Hamiltonian basis [106]. Consider the Hamiltonian:

$$H = e^{-\mu}\sum \frac{p_i^2}{2m} + e^{-\mu}\Phi(e^{\mu}\mathring{\mathbf{A}}) + e^{\mu}\frac{\bar{\eta}^2}{2Q_\eta} - 3e^{-\mu}Nk_BT_0\mu, \tag{94}$$

where the canonical variables $\bar{\mathbf{x}}$ and $\bar{\eta}$ are connected with the real variables $\mathbf{x}$ and η, respectively, through the transformations: $\mathring{\mathbf{A}} = e^{\mu}\mathbf{x}$ and $\bar{\eta} = e^{-\mu}Q_\eta\eta$. The Hamiltonian generates the equations of motion provided the constant of motion: $I = \sum p_i^2/2m + \Phi(\mathbf{x}) + 0.5Q_\eta\eta^2 + 3Nk_BT_0\mu = 0$, where $\mu = \int \eta dt$.

A strong form of Equation (92), where the virial of forces $\sum x_i\frac{\partial\Phi}{\partial x_i}$ is equal to $3Nk_BT_0$ at every time step, may be used to develop an isovirial thermostat [98]. The isovirial thermostat is analogous to the GIK thermostat but for the 'slow' configurational variables. The resulting dynamics, however, does not sample from a canonical distribution. The virial thermostat has not received widespread attention from researchers, and to the best of our knowledge, its applications have been limited to very small-scale systems. In our opinion, for larger systems, the virial thermostat is superior to the BT or the C_{12} thermostats, since the virial thermostat does not require the computation of the Hessian matrix.

7. Case studies

In this section, we subject the following systems – an SHO, a chain of anharmonic oscillators and a soft-sphere system – to the different thermostats in order to elucidate their features.

7.1. Equilibrium phase-space characteristics using an SHO

An SHO of unit mass and stiffness is kept in contact with a thermostat at $k_BT_0 = 1$. This pedagogical system serves as the best example to study the ergodic characteristics of a thermostat, and the relationship between the thermodynamic and dynamical quantities. The equations of motion are solved using the the 4^{th} order Runge-Kutta method where the incremental time step is chosen as 0.001.

Velocity Rescaling: The equations of motion of an SHO subjected to the velocity rescaling thermostat are:

$$\dot{x} = p, \quad \dot{p} = -x, \quad p \to 1. \tag{95}$$

Figure 2 depicts the phase-space trajectory when the rescaling is performed every 1000 time steps. As is evident, the trajectory fails to sample from the correct canonical ensemble (see Equation (11)). The phase-space trajectory is also dependent on the frequency of velocity rescaling.

Gaussian Isokinetic Thermostat: A GIK thermostatted SHO is governed by the following equations of motion:

$$\dot{x} = p, \ \dot{p} = 0, \ \lambda = \frac{-x}{p} \tag{96}$$

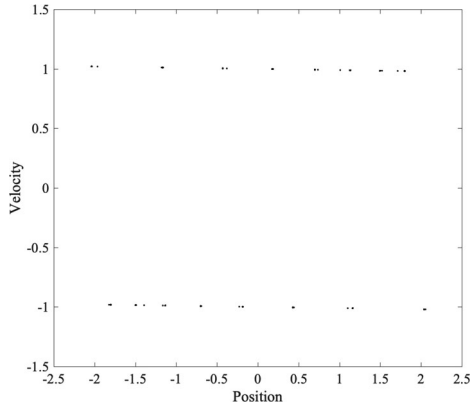

Figure 2. (Colour online) The phase space trajectory for the velocity-rescaling algorithm. The velocities are rescaled every 1000 time-steps. Notice that the velocity jumps between +1 and −1 depending on if the instantaneous velocity is positive or negative. It is clear that the dynamics does not sample from a canonical ensemble.

Without any numerical computation, the characteristics of the dynamics can be understood. Since $\dot{p} = 0$, the position of the oscillator keeps increasing, resulting in an unphysical situation. It is evident that for this problem, the GIK dynamics does not sample the configurational space canonically. Obtaining an isokinetic distribution requires the presence of *at least* two particles in the system. For even larger systems, it has been shown that a single GIK trajectory accurately samples from an isokinetic distribution [32].

Nosé Thermostat: The Nosé thermostat, with $Q_s = 1$, when coupled to an SHO, is governed by the equations:

$$\dot{x}' = \pi/s^2, \quad \dot{\pi} = -x', \quad \dot{s} = p_s', \quad \dot{p}_s' = \frac{1}{s}\left(\frac{\pi^2}{s^2} - 1\right). \tag{97}$$

Nosé dynamics represented by (97) is non-ergodic [17], and does not sample the phase space according to the canonical distribution. With initial conditions as $(x', \pi, s, p_s') = (1, 1, 1, 0)$, the phase space plot (see Figure 3(a)) indicates that the dynamics is limited to a torus and the distribution is not gaussian (see Figure 3(b)).

Nosé-Hoover Thermostat: Like the Nosé thermostat, the NH thermostat is also non-ergodic [17]. An SHO coupled to an

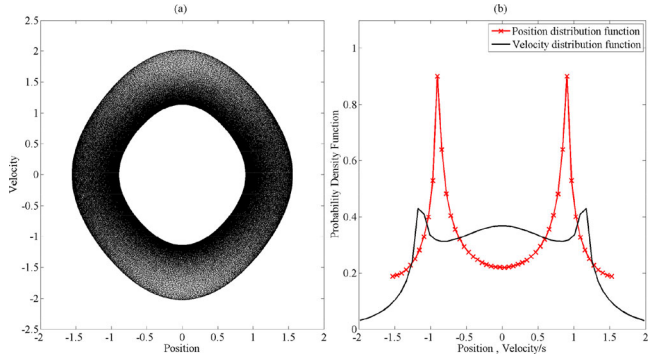

Figure 3. (Colour online) Non-ergodicity of Nosé dynamics for the initial condition $(x', \pi, s, p_s') = (1, 1, 1, 0)$ - (a) position-velocity plot of the oscillator and (b) probability distribution functions of the position and velocity/s. Notice the hole present in the dynamics in (a) and non-canonical nature of the distributions in (b).

NH thermostat with $Q_\eta = 1$ is governed by the equations of motion:

$$\dot{x} = p, \quad \dot{p} = -x - \eta p, \quad \dot{\eta} = \left(p^2 - 1\right). \tag{98}$$

The Poincaré section plot at $\eta = 0$ cross-section, for three different initial conditions, are shown in Figure 4: case (a) with $(x, p, \eta) = (1, 1, 0)$, case (b) with $(x, p, \eta) = (2, 2, 1)$, and case (c) $(x, p, \eta) = (3, 3, 3)$. For cases (a) and (b), two kneaded tori are obtained, while in case (c) the dynamics is chaotic. The plot clearly indicates that the phase-space can be easily partitioned into multiple non-communicating regions, and hence, the dynamics is not ergodic.

Although there is chaoticity in the dynamics for different initial conditions, the chaotic space makes up for only 6% of the entire phase-space [107]. In fact, none of the initial conditions sample the phase-space as per Equation (10). The poor ergodic characteristics of the NH thermostat may be explained by the periodic dynamics of the variable η [108], and the presence of conserved quantities that cause the energy of the system to be bounded [18].

Martyna-Klein-Tuckerman Thermostat: A two-variable MKT thermostatted SHO is governed by:

$$\begin{aligned} \dot{x} &= p, \quad \dot{p} = -x - \tfrac{\eta p}{Q_\eta}, \\ \dot{\eta} &= p^2 - 1 - \tfrac{\eta\xi}{Q_\xi}, \quad \dot{\xi} = \tfrac{\eta^2}{Q_\eta} - 1. \end{aligned} \tag{99}$$

The ergodic characteristics here are dependent on the choice of Q_η and Q_ξ [20,109,110]. For MKT thermostatted dynamics to be ergodic, the following conditional joint probability distribution functions (PDFs) hold true:

$$\begin{aligned} f(x, p|\eta = \eta_0, \xi = \xi_0) &\propto \exp\left(-\frac{x^2}{2}\right)\exp\left(-\frac{p^2}{2}\right) \\ f(\eta, \xi|x = x_0, p = p_0) &\propto \exp\left(-\frac{\eta^2}{2Q_\eta}\right)\exp\left(-\frac{\xi^2}{2Q_\xi}\right). \end{aligned} \tag{100}$$

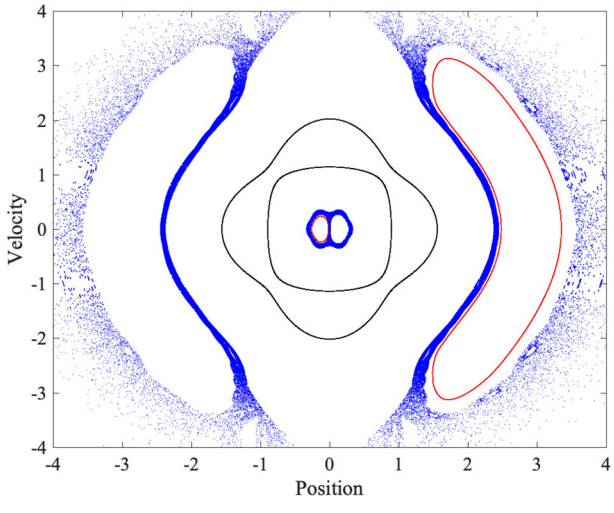

Figure 4. (Colour online) Poincaré section plots for the Nosé-Hoover dynamics at $\eta = 0$ cross-section for three different initial conditions: (a) black = $(x, p, \eta) = (1, 1, 0)$, (b) red = $(x, p, \eta) = (2, 2, 1)$, and (c) blue = $(x, p, \eta) = (3, 3, 3)$. The different initial conditions result in different nature of trajectories, with none being phase-space filling. The lack of ergodicity, and consequently the inability of NH thermostat to thermalise the SHO is self-evident.

The physical meaning of Equation (100) is that the joint PDF of x and p is a bivariate standard normal distribution at the Poincaré section $(\eta = \eta_0, \xi = \xi_0)$ while that of η and ξ is a bivariate normal distribution with variances equalling Q_η and Q_ξ, respectively, at the Poincaré section $(x = x_0, p = p_0)$.

As Q_η and Q_ξ deviate from unity, an appreciable difference is observed between the joint PDFs obtained from theory and numerical simulations. Figure 5 shows the Poincaré section plot at $|\eta| = |\xi| < 0.001$ cross-section for: (a) $Q_\eta = Q_\xi = 2$ and (b) $Q_\eta = Q_\xi = 10$. It is evident that in case (a) the dynamics is ergodic while in case (b) the dynamics is non-ergodic. Figure 6 shows the joint PDFs for these cases, where the difference from a joint normal distribution is clearly visible for $Q_\eta = Q_\xi = 10$. Rather than looking at the joint PDFs, if one looks at the marginal distributions, the dynamics *erroneously* looks ergodic even with $Q_\eta = Q_\xi = 10$ as can be seen in Figure 7.

An in-depth numerical investigation was performed by Hoover and coworkers [21] to understand the ergodic characteristics when $Q_\eta = Q_\xi = 1$. With millions of different initial conditions, they searched for an initial condition that results in a conservative hyper-dimensional torus. The resulting Lyapunov spectrum is: $\langle L_1\rangle = +0.066_5$, $\langle L_2\rangle = +0.000_0$, $\langle L_3\rangle = -0.000_0$, $\langle L_4\rangle = -0.066_5$ [21], with none of the initial conditions resulting in statistically significant deviation from these values. Thus, it can be concluded that with $Q_\eta = Q_\xi = 1$, the ergodic characteristics of the MKT thermostat become superior to the NH thermostat.

The results emphasise the importance of correctly choosing Q_η and Q_ξ while studying the MKT thermostatted dynamics in

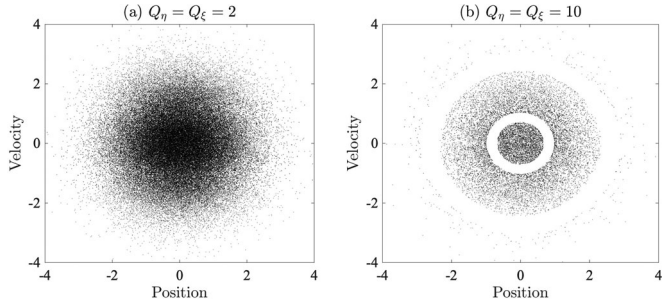

Figure 5. (Colour online) Poincaré section at $|\eta| = |\xi| < 0.001$ cross-section for: (a) $Q_\eta = Q_\xi = 2$ and (b) $Q_\eta = Q_\xi = 10$. As is evident, for case (b) the dynamics is non-ergodic while for case (a) the dynamics is ergodic.

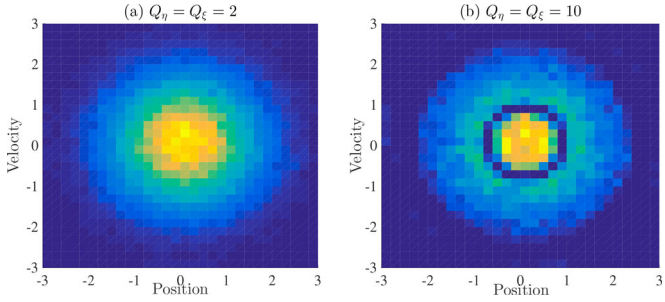

Figure 6. (Colour online) Joint PDF of MKT thermostatted oscillator at the Poincaré section given by $|\eta| = |\xi| < 0.001$ with: (a) $Q_\eta = Q_\xi = 2$ and (b) $Q_\eta = Q_\xi = 10$. The deviation from normality is obvious in case (b).

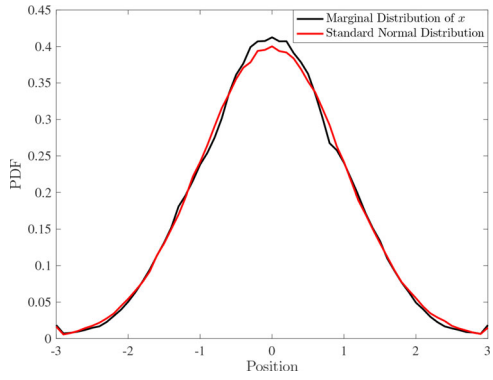

Figure 7. (Colour online) Marginal distribution of x obtained by projecting all trajectory points and its comparison with a standard normal distribution. Notice the good agreement between the two distributions. A similar conclusion can be reached from the marginal distribution of p as well.

a small-scale system. Some questions still remain open, though, – for what values of Q_η and Q_ξ, the dynamics of an MKT thermostatted oscillator is ergodic, and the exact value of Q_η and Q_ξ at which the stable periodic orbit disappears.

Hoover-Holian Thermostat: Now let us look at the phase-space characteristics of the HH thermostatted SHO. An equivalent form of the equations of motion, for this case, are:

$$\begin{aligned} \dot{x} &= p, \quad \dot{p} = -x - \eta p - \xi p^3, \\ \dot{\eta} &= \tfrac{1}{Q_\eta}\left(p^2 - 1\right), \quad \dot{\xi} = \tfrac{1}{Q_\xi}\left(p^4 - 3p^2\right). \end{aligned} \tag{101}$$

Choosing $Q_\eta = Q_\xi = 1$ results in a scenario where the oscillator comes to thermal equilibrium at a temperature of unity, and the extended phase-space distribution becomes a product of four independent standard normal variables. The HH thermostatted SHO correctly samples the phase-space from a canonical distribution both in the projected space as well as at Poincaré sections, similar to the MKT thermostatted SHO with $Q_\xi = Q_\eta \to 1$, and hence, not shown here.

The marginal distribution of x at the Poincaré section of $|\eta| = |\xi| < 0.001$ has been plotted in Figure 8. The results correspond to the initial conditions $(x, p, \eta, \xi) = (1, 0, 0, 0)$. The equivalence of the PDF with that of a standard normal PDF

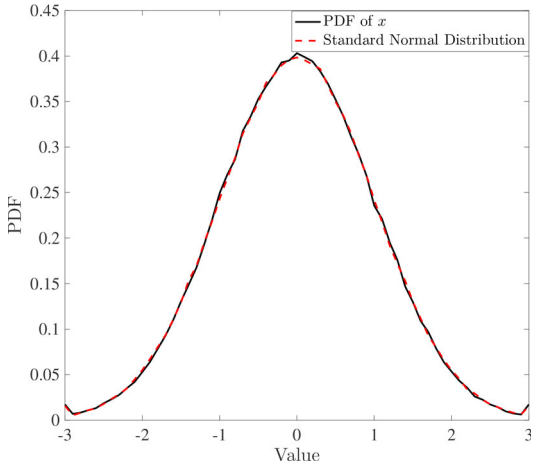

Figure 8. (Colour online) PDF of x of the HH thermostatted SHO at the Poincaré section $|\eta| = |\xi| < 0.001$ when it is subjected to $k_B T_0 = 1$. The initial conditions are $(x, p, \eta, \xi) = (1, 0, 0, 0)$. Notice the good agreement of the PDF of x with the standard normal distribution.

suggests that that the HH thermostat is ergodic from statistical perspective.

A similar conclusion can also be reached from the dynamical perspective. Working with millions of different initial conditions, Hoover and coworkers [21] made an exhaustive search for an initial condition that would result in a conservative hyper-dimensional torus. Their findings suggest that no initial condition within their search domain results in the Lyapunov spectrum to be different from the average Lyapunov spectrum: $\langle L_1 \rangle = +0.068_0, \langle L_2 \rangle = +0.000_0, \langle L_3 \rangle = -0.000_0, \langle L_4 \rangle = -0.068_0$. But, it must be noted that this brute-force method of ascertaining ergodicity is not *full proof*, and there may still exist an initial condition for which the largest Lyapunov exponent is zero.

Campisi-Zhan-Talkner-Hängii Thermostat: When the SHO is coupled to a log thermostat through a Hookean spring $h(x, s) = 0.5k(x - s)^2$, the equations of motion are:

$$\begin{aligned} \dot{x} &= p, \quad \dot{p} = -x - k(x - s), \\ \dot{s} &= p_s, \quad \dot{p}_s = \tfrac{s}{s^2 + \delta} + k(x - s). \end{aligned} \tag{102}$$

The phase-space characteristics for different choice of the parameters k and δ are shown in Figure 9 : black – $k = 0.1, \delta = 0.001$, red – $k = 0.1, \delta = 0.01$, blue – $k = 0.01, \delta = 0.001$, and green – $k = 0.01, \delta = 0.01$. Notice that none of the cases resulted in a situation where the entire phase-space is filled. Consequently, the dynamics is not ergodic.

The dependence of the phase-space characteristics on the choice of the coupling function and the magnitude of k presents a problem – as the coupling function changes, the dynamical properties change as well. The choice of a good coupling function remains an area open to research.

Patra-Bhattacharya Thermostat: We now subject the SHO to the PB thermostat to show that it is non-ergodic. If the thermostat masses are such that $Q_\eta = Q_\xi = 1$, the equations of motion are given by:

$$\begin{aligned} &\dot{x} = p - \xi x, \quad \dot{p} = -x - \eta p, \quad \dot{\eta} = p^2 - 1.0, \\ &\dot{\xi} = x^2 - 1.0 \end{aligned} \tag{103}$$

Numerically solving these equations shows the presence of hyper-dimensional tori distributed within a chaotic sea. The double Poincaré section plot at $|\eta| = |\xi| < 0.001$ for three different initial conditions are shown in Figure 10:

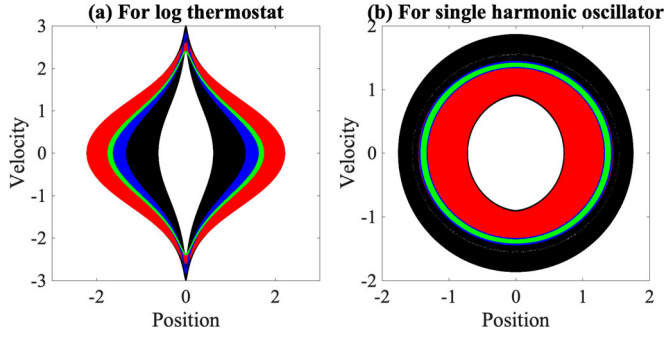

Figure 9. (Colour online) Plot of position and velocity for: (a) log thermostat and (b) SHO. The different colours correspond to: black – $k = 0.1, \delta = 0.001$, red – $k = 0.1, \delta = 0.01$, blue – $k = 0.01, \delta = 0.001$, green – $k = 0.01, \delta = 0.01$. Notice that for none of the cases, the trajectory of the SHO is such that the entire phase-space is filled. Consequently, the dynamics is not ergodic.

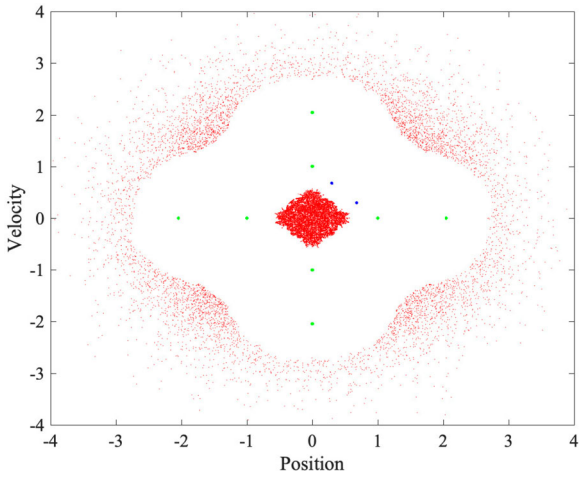

Figure 10. (Colour online) Plot of position and velocity of the Patra-Bhattacharya thermostatted SHO at the double Poincaré section $|\eta| = |\xi| < 0.001$ for three different initial conditions: green – $(x, p, \eta, \xi) = (1, 0, 0, 0)$, red – $(x, p, \eta, \xi) = (4, 1, 0, 0)$ and blue – $(x, p, \eta, \xi) = (0, 1, 0, 1)$. The trajectories corresponding to green and blue colours are such that hyper-dimensional tori are formed, while that corresponding to red is chaotic. However, the entire phase-space is not filled by a single trajectory, and consequently, the dynamics is non-ergodic.

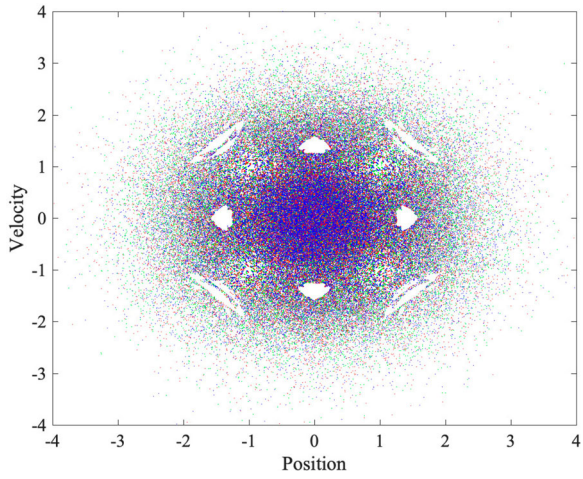

Figure 11. (Colour online) Plot of position and velocity for the Bauer-Bulgac-Kusnezov thermostatted SHO at the double Poincaré section $|\xi| = |\eta| < 0.001$ for three different initial conditions: green – $(x, p, \eta, \xi) = (1, 0, 0, 0)$, red – $(x, p, \eta, \xi) = (4, 1, 0, 0)$ and blue – $(x, p, \eta, \xi) = (0, 1, 0, 1)$. Although all trajectories are chaotic, the entire phase-space is not filled by a single trajectory, and consequently, the dynamics is non-ergodic. Note, however, that the ergodic characteristics have shown a marked improvement over the Patra-Bhattacharya thermostat for the same initial conditions.

green – $(x, p, \eta, \xi) = (1, 0, 0, 0)$, red – $(x, p, \eta, \xi) = (4, 1, 0, 0)$ and blue – $(x, p, \eta, \xi) = (0, 1, 0, 1)$. The trajectories corresponding to green and blue dots represent hyper-dimensional tori, while that corresponding to red is chaotic. Clearly, for none of these three initial conditions the dynamics samples from the distribution

$$f_{\text{ex}}(x, p, \eta, \xi) \propto e^{-\left[\frac{x^2}{2}+\frac{p^2}{2}+\frac{\eta^2}{2}+\frac{\xi^2}{2}\right]}, \tag{104}$$

and hence, is not ergodic. Further, the phase-space can be partitioned into non-communicating regions and the entirety of the phase-space is not accessible from a single trajectory.

Bauer-Bulgac-Kusnezov Thermostat: As discussed previously, the BBK thermostat provides improved ergodic characteristics than either the NH or the PB thermostat. We will deal with the specific case of cubic coupling, for which, the SHO has the following equations of motion:

$$\begin{aligned} \dot{x} &= p - \xi^3 x, \quad \dot{p} = -x - \eta^3 p, \\ \dot{\eta} &= \tfrac{1}{Q_\eta}\left[p^2 - 1\right], \quad \dot{\xi} = \tfrac{1}{Q_\xi}\left[x^2 - 1\right]. \end{aligned} \tag{105}$$

Choosing $Q_\xi = Q_\eta = 1$, the equations have a stark resemblance with the PB thermostatted SHO. However, in presence of cubic coupling the SHO is able to sample more allowable phase-space as the cubic nature of the coupling aids in phase-space mixing.

For the same initial conditions chosen for the PB thermostat, the BBK thermostatted oscillator shows improved ergodic characteristics, as shown in Figure 11.

Note that the extended phase-space density for this specific coupling type is given by:

$$f_{\text{ex}} \propto \exp\left[-\left(\frac{p^2}{2}+\frac{x^2}{2}+\frac{\xi^4}{4}+\frac{\eta^4}{4}\right)\right]. \tag{106}$$

So, the dynamics is still not ergodic with the cubic coupling. However, the BBK formalism allows the development of arbitrary coupling functions that could result in an ergodically thermostatted SHO.

Braga-Travis / Virial and C_{12} Thermostats: For the SHO coupled with the BT thermostat, the equations of motion are:

$$\dot{x} = p - \xi x, \quad \dot{p} = -x, \quad \dot{\xi} = \frac{1}{Q_\xi}\left[x^2 - 1\right]. \tag{107}$$

These equations of motion bear stark resemblance with the NH thermostatted SHO (having x and p interchanged). So, similar to the NH thermostat, the BT thermostat displays non-ergodicity. The Poincaré section plot at $|\xi| < 0.001$ with $Q_\xi = 1$ is shown for three initial conditions in the Figure 12. Again, as expected, the Poincaré section plots are similar to that of the NH thermostat, with x and p interchanged. Due

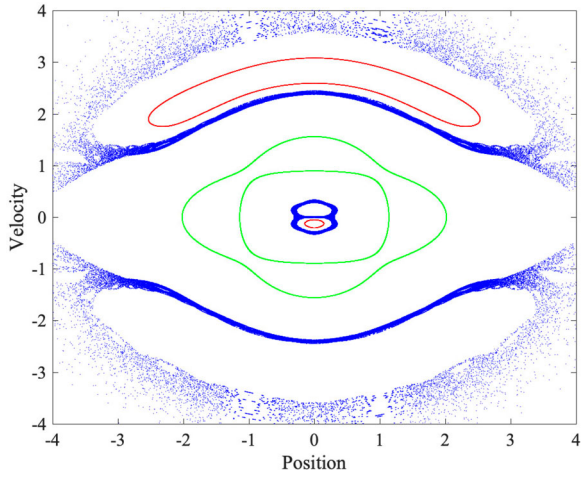

Figure 12. (Colour online) Poincaré section plots for the Braga-Travis dynamics at $|\xi| < 0.001$ cross section for three different initial conditions: (a) green = $(x, p, \eta) = (1, 1, 0)$, (b) red = $(x, p, \eta) = (2, 2, 1)$, and (c) blue = $(x, p, \eta) = (3, 3, 3)$. The different initial conditions result in different nature of trajectories, with none being phase-space filling. These figures are reminiscent of the Nosé-Hoover dynamics with x and p interchanged. Like the Nosé-Hoover thermostat, the lack of ergodicity, and consequently the inability of Braga-Travis thermostat to thermalise the SHO is self evident.

to the similarity with the NH thermostatted SHO, all discussions on the NH thermostatted SHO are valid for the BT thermostatted SHO as well. Note that the SHO thermostatted using the Virial thermostat is identical to the equations of motion (107), and hence, not probed any further.

The SHO coupled with the C_{12} thermostat is defined by the equations of motion:

$$\begin{aligned} \dot{x} &= p - \eta x - \xi x^3, \quad \dot{p} = -x, \\ \dot{\eta} &= \frac{1}{Q_\eta}\left(x^2 - 1\right), \quad \dot{\xi} = \frac{1}{Q_\xi}\left(x^4 - 3x^2\right). \end{aligned} \tag{108}$$

Assuming, $Q_\eta = Q_\xi = 1$, the dynamics bears resemblance with the HH thermostatted oscillator. The dynamics, therefore, has similar ergodic properties like the HH thermostat as well. The non-ergodicity observed with the BT thermostat disappears under the C_{12} thermostat.

From the equilibrium response of an SHO, we see that some of the thermostats behave similarly – the BT and the C_{12} thermostats are equivalent to the NH and the HH thermostats, respectively. Likewise, the virial thermostat is identical to the BT thermostat. When it comes to ergodic thermostats – the HH, the MKT and the C_{12} thermostats – the phase-space properties are non-distinguishable. However, the scenario will change in non-equilibrium cases, which we look next.

7.2. Non-equilibrium phase-space characteristics using an SHO

In order to understand robust heat flow in an SHO, we subject the SHO to a position-dependent temperature field, as shown in Equation (13). As has been explained previously, a robust heat flow is associated with the loss of phase-space volume, and therefore, serves as the check of the Second Law of thermodynamics. The governing equations of motion of the thermostatted oscillator remain the same as that in the equilibrium case, with the exception of the position-dependent temperature. The equations are integrated using the the 4^{th} order Runge-Kutta method with an incremental time step of 0.001.

Gaussian Isokinetic Thermostat: When subjected to a position-dependent temperature field with $\epsilon = 0.1$, the GIK thermostatted shows an unstable behaviour, as can be seen in Figure 13. With the initial conditions chosen as $(x, p) = (0, 1)$, the instability occurs primarily because of the large feedback from the Lagrange multiplier $\lambda = -xp/(1 + 0.1\tanh(x))$. As will be evident from the later case studies, the instabilities disappear for larger systems.

Nosé-Hoover Thermostat: We now couple the SHO with the NH thermostat. The resulting equations of motion according to Equations (49) and (57) with $Q_\eta = 1$, are, respectively:

$$\begin{aligned} \dot{x} &= p, \quad \dot{p} = -x - \eta p, \quad \dot{\eta} = \left(p^2 - k_B T(x)\right); \\ \dot{x} &= p, \quad \dot{p} = -x - \eta p, \quad \dot{\eta} = \left(\frac{p^2}{k_B T(x)} - 1\right). \end{aligned} \tag{109}$$

where, $k_B T(x) = 1.0 + 0.30\tanh(x)$. The two equations of motion enable us to illustrate the situation where the thermodynamic quantities are in agreement with the dynamical quantities. We use the same initial conditions as that in the equilibrium SHO case. The phase-space portrait, at the Poincaré section defined by $\eta = 0$, is shown in Figure 14. The plots differ from that of equilibrium as well as with each other.

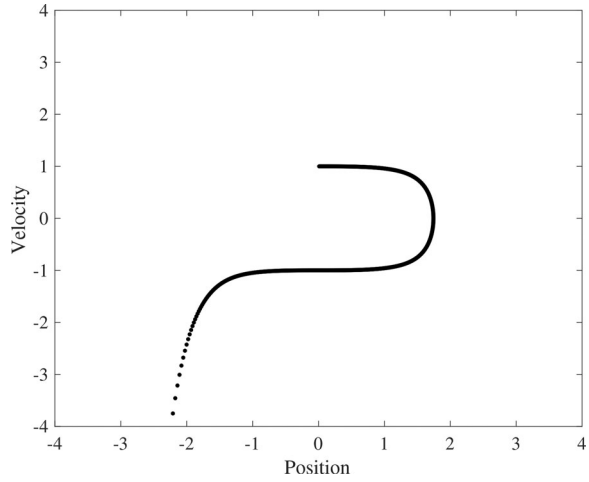

Figure 13. (Colour online) Instability in dynamics of GIK thermostatted oscillator when subjected to a position-dependent temperature field. The initial conditions are: $(x, p) = (0, 1)$. Because of the large feedback from the GIK multiplier λ, the dynamics becomes unstable.

The different thermodynamic quantities, for the two types of evolution and the three initial conditions, are summarised in Table 1. In stationary states, when net work is absent, the total time-averaged rate of heat flow must vanish, which implies $\langle \dot{Q} \rangle = 0$. The results indicate that all cases satisfy this fundamental argument. However, some of the NH trajectories are conservative for which $\langle \dot{S} \rangle = \langle \Lambda \rangle = 0$, while others are dissipative for which $\langle \dot{S} \rangle = \langle \Lambda \rangle < 0$. This is evident from the

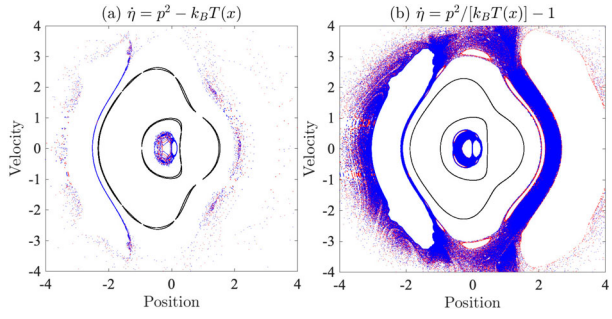

Figure 14. (Colour online) Poincaré plot of Nosé-Hoover dynamics subjected to a position dependent temperature field: $k_B T(x) = 1 + 0.30\tanh(x)$ at the cross-section $\eta \in [-0.001, 0.001]$ for three initial conditions: black = $(x, p, \eta) = (1, 1, 0)$, red = $(x, p, \eta) = (2, 2, 1)$, and blue = $(x, p, \eta) = (3, 3, 3)$. Figure (a) corresponds to the evolution where $\dot{\eta} = (p^2 - k_B T(x))$, while figure (b) is for the evolution where $\dot{\eta} = (p^2/[k_B T(x)] - 1)$.

Table 1. Different thermodynamic quantities for the three sets of initial conditions: black = $(x, p, \eta) = (1, 1, 0)$, red = $(x, p, \eta) = (2, 2, 1)$, and blue = $(x, p, \eta) = (3, 3, 3)$. $\langle \dot{Q} \rangle$ denotes the average rate of heat flow, $\langle \dot{S} \rangle$ is the average rate of heat-flow entropy and $\langle \Lambda \rangle$ is the average phase-space compression. Each quantity has a subscript: $_T$ denotes the equations of motion with $\dot{\eta} = (p^2 - k_B T(x))$, while $_B$ is for the evolution with $\dot{\eta} = (p^2/[k_B T(x)] - 1)$. Notice that while $\langle \dot{S}_T \rangle \neq \langle \Lambda_T \rangle$, $\langle \dot{S}_B \rangle = \langle \Lambda_B \rangle$, as has been discussed in the text.

	$\langle \dot{Q}_T \rangle$	$\langle \dot{Q}_B \rangle$	$\langle \dot{S}_T \rangle$	$\langle \dot{S}_B \rangle$	$\langle \Lambda_T \rangle$	$\langle \Lambda_B \rangle$
Set (a)	0.0000	0.0000	0.0000	0.0000	0.0000	0.0000
Set (b)	0.0000	0.0000	−0.0061	−0.0002	−0.0114	−0.0002
Set (c)	0.0000	0.0000	−0.0061	−0.0002	−0.0113	−0.0002

phase-space plot as well – the conservative trajectory with a three-dimensional torus occurs for initial conditions $(x, p, \eta) = (1, 1, 0)$ while dissipative trajectories occur for the remaining two initial conditions. The co-existence of the conservative and the dissipative features [12] is a unique feature of the NH dynamics which occurs due to its non-ergodicity. The time-averaged heat-flow entropy rate agrees with the average phase-space compression only under the evolution $\dot{\eta} = (p^2/[k_BT(x)] - 1)$, as has been discussed previously.

Martyna-Klein-Tuckerman Thermostat: We now subject the SHO to the two-chain MKT thermostat with $Q_\eta = Q_\xi = 1$ and $k_BT(x) = 1.0 + 0.2\tanh(x)$. Like the NH thermostat, two sets of equations of motion can be written – (i) the usual equations of motion, where $\langle \dot{S}/k_B \rangle \neq -\langle \Lambda \rangle$ (Set 1):

$$\begin{aligned} \dot{x} &= p, \quad \dot{p} = -x - \eta p, \\ \dot{\eta} &= p^2 - k_BT(x) - \eta\xi, \quad \dot{\xi} = \eta^2 - k_BT(x), \end{aligned} \tag{110}$$

and (ii) the modified equations of motion, where $\langle \dot{S}/k_B \rangle = -\langle \Lambda \rangle$ (Set 2):

$$\begin{aligned} \dot{x} &= p, \quad \dot{p} = -x - \eta p, \\ \dot{\eta} &= p^2/[k_BT(x)] - 1 - \eta\xi, \quad \dot{\xi} = \eta^2 - 1, \end{aligned} \tag{111}$$

The Poincaré section plots at the cross-section $|\eta| = |\xi| < 0.001$ are shown in Figure 15. Notice that the phase-space filling nature of the equilibrium dynamics has given way to a complicated multi-fractal for both the equation sets. The presence of such a multi-fractal is a signature of satisfying the Second Law of thermodynamics [111–114].

For the two sets, the different thermodynamic variables are summarised in Table 2. The time-averaged Lyapunov exponents are: $\langle L_1 \rangle = 0.069_2$, $\langle L_2 \rangle = 0$, $\langle L_3 \rangle = -0.015_9$, $\langle L_4 \rangle = -0.085_6$ such that $\sum \langle L_i \rangle < 0$. The negative sum indicates that the phase-space volume has contracted and the Kaplan-Yorke dimension (= 3.624), which is calculated by linearly interpolating between the last positive sum of Lyapunov exponents and the first negative sum, is not equal to the embedding dimension (= 4.0). Thus, the MKT thermostat has improved ergodic characteristics along with the ability to show phase-space compression and heat flow in non-equilibrium. Its ease of implementation has made the MKT thermostat very popular for investigating a variety of equilibrium and non-equilibrium situations. In fact, the two-chain MKT thermostat is now a standard library function in several well-known MD software such as LAMMPS [115], Gromacs [116], etc.

Hoover-Holian Thermostat: The equilibrium properties of the HH thermostat are identical to that due to the MKT thermostat. However, in presence of the position-dependent temperature field: $k_BT(x) = 1.0 + 0.2\tanh(x)$, the differences start to emerge. The equations of motion of the HH thermostat in this case is identical to that of the equilibrium SHO equations with temperature replaced by $k_BT(x)$.

As is expected from a good thermostat, Figure 16 shows that under the imposed temperature field, the dynamics is multi-fractal. The presence of a multi-fractal is a signature of the information dimension being smaller than the embedding dimension (in this case 4) and conformity with the Second Law of thermodynamics. A comparison with the MKT thermostatted SHO suggests that the: (i) the nature of the multi-fractal is significantly different for the HH thermostatted SHO (see Figure 15), (ii) the spectrum of Lyapunov exponents, which in the case of HH thermostatted SHO is: $\langle L_1 \rangle = +0.065_0$, $\langle L_2 \rangle = +0.000_3$, $\langle L_3 \rangle = -0.001_2$, $\langle L_4 \rangle = -0.070_2$, is different, and (iii) the Kaplan-Yorke dimension is 3.913, which is different as well. These differences make us ask the question – which of the two thermostats result in a closer approximation of reality. The question remains open for answering.

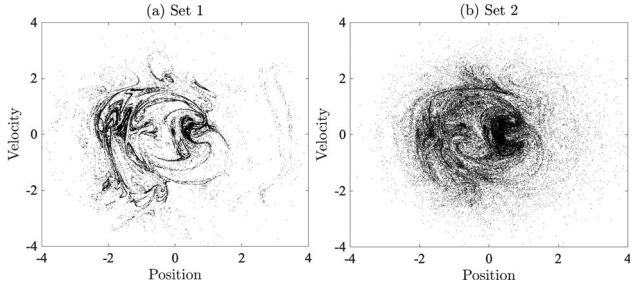

Figure 15. (Colour online) Poincaré section plot of the Martyna-Klein-Tuckerman thermostatted oscillator subjected to the position dependent temperature field: $k_BT(x) = 1 + 0.2\tanh(x)$ at the cross-section $|\eta| = |\xi| < 0.001$. The initial conditions are $(x, p, \eta, \xi) = (1, 0, 0, 0)$. Notice that the multifractal nature of the dynamics. The multifractal nature indicates that the phase-space volume has 'shrunk'.

Table 2. Different thermodynamic quantities for the two equation sets with initial conditions $(x, p, \eta, \xi) = (1, 0, 0, 0)$. Each quantity has a subscript: $_1$ denotes the equations of motion (110), while $_2$ is for the denotes the equations of motion (111). Notice that while $\langle \dot{S}_1 \rangle \neq \langle \Lambda_1 \rangle$, $\langle \dot{S}_2 \rangle = \langle \Lambda_2 \rangle$.

$\langle \dot{Q}_1 \rangle$	$\langle \dot{Q}_2 \rangle$	$\langle \dot{S}_1 \rangle$	$\langle \dot{S}_2 \rangle$	$\langle \Lambda_1 \rangle$	$\langle \Lambda_2 \rangle$
0.0000	0.0000	−0.0164	−0.0038	−0.0322	−0.0038

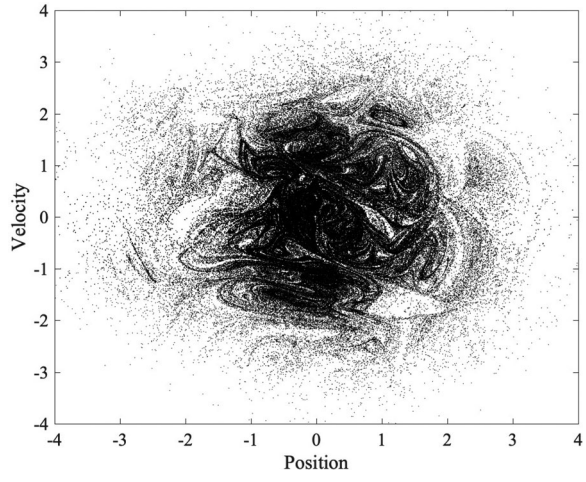

Figure 16. (Colour online) Poincaré section plot of the Hoover-Holian thermostatted oscillator subjected to the position dependent temperature field: $T(x) = 1 + 0.2\tanh(x)$ at the cross-section $|\eta| = |\xi| < 0.001$. The initial conditions are $(x, p, \eta, \xi) = (1, 0, 0, 0)$. The dynamics is multifractal like the MKT thermostatted oscillator, but the nature of the multifractal is different. Additionally, $\langle \Lambda \rangle$ and the information dimension of the multifractal are different from those of the MKT thermostatted oscillator.

Patra-Bhattacharya Thermostat: A robust heat flow is obtained in the PB thermostatted SHO as well when $k_B T(x) = 1 + 0.2\tanh(x)$. However, due to non-ergodicity, not all initial conditions result in dissipative trajectories – conservative trajectories co-exist with dissipative trajectories, especially when ε is small. For the same initial conditions as that in the equilibrium case, the double Poincaré section is shown in Figure 17. The multifractal nature of the dynamics is evident, suggesting a robust heat flow.

Due the similarity of the response, the remaining thermostats are not discussed.

7.3. A Φ^4 chain under thermal conduction

So far the two case studies discussed involve a system comprising a single particle. While these case studies are quite instructive and allow easy reproduction of the results, MD simulations typically involve several thousand particles. Therefore, we now look a relatively larger system of a one-dimensional Φ^4 chain comprising N=256 particles. The chain comprises N particles, each of mass m, arranged on a one-dimensional line and separated by a distance l_{eq}, as depicted in Figure 18. Each particle is connected with its nearest neighbour by means of a harmonic spring and to its initial equilibrium position by a quartic tethering spring. As a result, the harmonic and tethering potentials take the form: $V_H(\Delta x_{i-1,i}) = \frac{1}{2}k(x_{i-1} - x_i - l_{eq})^2$ and $U(x_i) = \frac{1}{4}c(x_i - x_{i,0})^4$, respectively. Here, x_i and $x_{i,0}$ are the instantaneous and equilibrium positions of the i^{th} particle, respectively. The boundary conditions may be taken as fixed, wherein a fixed particle of similar characteristics is placed at the either ends, or periodic, wherein the N^{th} particle is connected with the first particle. For a Φ^4 chain with fixed boundaries, and $m = k = l_{eq} = 1.0$, the Hamiltonian becomes:

$$H_{\Phi^4} = \sum_{i=1}^{N}\left[\frac{p_i^2}{2}\right] + \sum_{i=1}^{N+1}\left[\frac{1}{2}(x_i - x_{i-1} - 1.0)^2\right] + \sum_{i=1}^{N}\left[\frac{c}{4}(x_i - x_{i,0})^4\right]. \tag{112}$$

Note that $x_0 = -1$ and $x_{N+1} = N$, and these boundary particles remain fixed to their initial coordinates throughout the simulation.

The first and the last 25 particles (=N_T) of the chain are subjected to two thermostats kept at different temperatures (T_H and T_C, where $T_H > T_C$). The middle particles evolve according to the standard Newtonian evolution. For any of these middle site i, the instantaneous local heat current can be obtained from the time derivative of the local energy density, ϵ_i, [117]:

$$\dot{\epsilon}_i = \frac{\partial \epsilon_i}{\partial t} + \left[j_{i-1,i} - j_{i,i+1}\right]. \tag{113}$$

In Equation (113), $j_{i,j}$ represents the energy current flowing from the i^{th} to the j^{th} particle:

$$j_{i,j} = \frac{1}{2}\left[f_{i,j}(v_i + v_j)\right], \tag{114}$$

where $f_{i,j}$ is force acting on the j^{th} particle due to the ith particle. At steady-state, Equation (113) simplifies to $\langle j_{i-1,i}\rangle = \langle j_{i,i+1}\rangle$ and Equation (114) becomes:

$$\langle j_{i-1,i}\rangle = \langle \frac{1}{2}(v_i + v_{i-1}) f_{i-1,i}\rangle = \langle v_i f_{i-1,i}\rangle. \tag{115}$$

The time averaged value of heat flux, $\langle J\rangle$, may now be computed as:

$$\langle J\rangle = \left\langle \frac{\sum_{i=N_T}^{N-N_T} j_{i,i-1}}{N - 2N_T} \right\rangle, \tag{116}$$

from which the thermal conductivity, κ, is given by:

$$\kappa = \frac{\langle J\rangle (N - 2N_T)}{\Delta T}. \tag{117}$$

Here, $\Delta T/(N - 2N_T)$ is the temperature gradient with

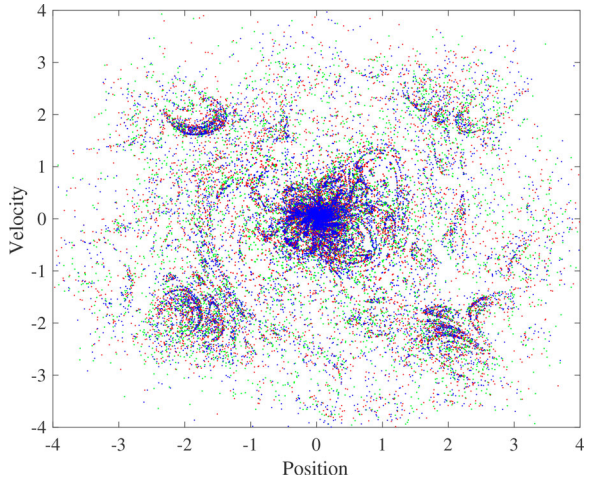

Figure 17. (Colour online) Plot of position and velocity of the Patra-Bhattacharya thermostatted SHO at the double Poincaré section $|\eta| = |\xi| < 0.001$ for three different initial conditions: green – $(x, p, \eta, \xi) = (1, 0, 0, 0)$, red – $(x, p, \eta, \xi) = (4, 1, 0, 0)$ and blue – $(x, p, \eta, \xi) = (0, 1, 0, 1)$. The multifractal nature of the dynamics is evident suggesting a robust heat flow in the Patra-Bhattacharya thermostatted oscillator.

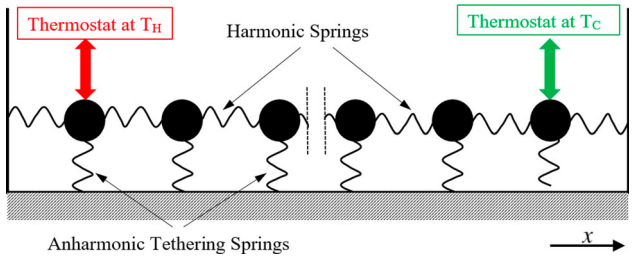

Figure 18. (Colour online) Pictorial representation of a Φ^4 chain subjected to two thermostats at the end. The anharmonic springs tether the particles to their equilibrium positions and provide force only along the x direction.

Table 3. Thermal conductivity, κ, due to the different thermostats and different ΔT.

ΔT	Rescale	GIK	NH	MKT	HH	PB	BT	BBK
0.2	2.481	2.732	2.645	2.630	2.682	2.727	2.594	2.743
0.5	2.727	2.678	2.707	2.678	2.682	2.796	2.628	2.684
1.0	2.910	2.941	2.848	2.906	2.857	2.995	2.941	2.986

$\Delta T = T_H - T_C$. Our results for κ,shown in Table 3, suggests that κ can be clustered into three distinct groups depending on the type of temperature being controlled. For example, the kinetic temperature controlling thermostats (NH, MKT and HH) provide similar κ at different ΔT values. Likewise, the two full phase-space thermostats (PB and BBK) result in similar values of κ. The κ due to the configurational BT thermostat is different from that of the kinetic or the full phase-space thermostats. Unlike the cases involving SHO, the differences between the different kinetic (or configurational or full phase-space) thermostats disappear for this large system and the results are comparable. This is because the effect of non-ergodicity is superseded by the (prohibitively) large Poincaré recurrence time for this moderately large system.

While κ for the velocity rescaling and the GIK thermostats are not too different from the other kinetic temperature based thermostats, the temperature profiles due to these two thermostats show unphysical jumps, as can be seen in Figure 19. The jumps are present when $\Delta T \to 0$. The similarity between the values of κ occurs because of the similarity of the temperature gradient.

It appears to us that the full phase-space thermostats should be preferred over either the kinetic or the configurational thermostats for studying thermal conduction. Apart from providing results as per expectation for κ and kinetic temperature profiles, the full phase-space thermostats offer an additional advantage over the other thermostats – the equality of the kinetic and the configurational temperatures locally in problems related to thermal conduction [118,118].

7.4. Planar shear flow

We now study a different class of non-equilibrium problem wherein the system is subjected to a planar shear flow. This problem is amongst the first to be studied through homogeneous non-equilibrium MD (NEMD) simulations. Consider a 2-dimensional system comprising N=625 particles and subjected to a planar shear flow along the x direction. The simulation box is a square whose each side equals L=25 units. The particles are initially placed on a square lattice such that the distance between the nearest neighbour is 1 units. Let the particles of the system interact through the soft-sphere potential:

$$\Phi(r_{ij}) = 100(1 - r_{ij}^2)^4; r_{ij}^2 = (x_j - x_i)^2 + (y_j - y_i)^2, \quad (118)$$

when $r_{ij} \leq 1$ and $\Phi(r_{ij}) = 0$ for $r_{ij} > 1$. Under the planar shear flow, the velocity gradient of a particle has the form:

$$\nabla \mathbf{u} = \begin{pmatrix} 0 & 0 \\ \dot{\gamma} & 0 \end{pmatrix}, \quad (119)$$

where, $\dot{\gamma}$ is the shear rate that drives the system. Assuming the mass of each particle to be unity, the SLLOD equations of motion for simulating the planar flow in the absence of a thermostat are:

$$\begin{aligned} \dot{x}_i &= p_{x,i} + y_i \dot{\gamma} \\ \dot{p}_{x,i} &= F_{x,i} - p_{y,i} \dot{\gamma} \\ \dot{y}_i &= p_{y,i} \\ \dot{p}_{y,i} &= F_{y,i} \end{aligned} \quad (120)$$

Note that here the momenta p are peculiar with respect to the hydrodynamic streaming velocity $u = u(y)$ in x-direction. To ensure homogeneity, periodic boundary conditions formulated by Lees and Edwards [120] need to be adopted. Appropriate modifications to the minimum image convention also need to be incorporated. In absence of thermostats, the shear flow is adiabatic with continuous heating. Therefore, a thermostat is necessary to ensure a steady state.

In the limit, $\dot{\gamma} \to 0$, the NEMD results may be post-processed for calculating the shear viscosity, μ:

$$\mu = \lim_{t\to\infty} \lim_{\dot{\gamma}\to 0} -\frac{\langle P_{xy} \rangle}{\dot{\gamma}}, \quad (121)$$

where, $\langle \ldots \rangle$ denotes time average, and P_{xy} is the off-diagonal (xy) term of the pressure tensor:

$$P_{xy} = \frac{1}{L^2} \sum_{i=1}^{N} \left[p_{x,i} p_{y,i} + \sum_{j<i} F_{x,ij} y_{ij} \right]. \quad (122)$$

Note that $F_{x,ij}$ denotes the x component of the force acting on the particle i due to the particle j, and $y_{ij} = y_j - y_i$.

When coupled with four different thermostats – the GIK, the NH, the PB and the BT thermostats, the equations of motion get modified accordingly. We integrate these equations of motion for 5 million time steps using the 4th order Runge-Kutta method with $\Delta t = 0.001$, of which the last 2.5 million time steps have been taken as the production runs. The results of $\langle P_{xy} \rangle$ for different values of $\dot{\gamma}$ are shown in the Table 4. At smaller $\dot{\gamma}$, $\langle P_{xy} \rangle$ due to the different thermostats agree with

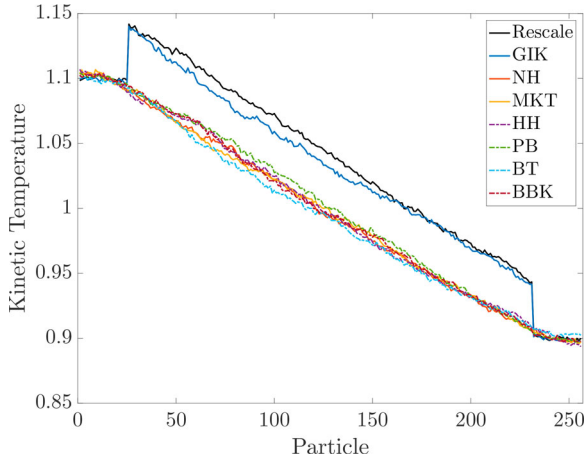

Figure 19. (Colour online) The temperature profile due to the different thermostats when $\Delta T = 0.20$. Notice the jumps at the boundaries between the thermostatted and the non-thermostatted particles.

Table 4. The time averaged value of the xy component of the pressure tensor, $\langle P_{xy} \rangle$, for the different thermostats at different $\dot{\gamma}$. At smaller $\dot{\gamma}$, P_{xy} due to the different thermostats agree with each other. With increasing $\dot{\gamma}$, the disparity between the thermostats increase.

$\dot{\gamma}$	GIK	NH	PB	BT
0.5	−0.647	−0.645	−0.637	−0.640
1.0	−1.121	−1.210	−1.178	−1.194
5.0	−2.473	−2.527	−3.603	−4.964

each other, and match with previously reported values [121]. However, as $\dot{\gamma}$ increases, the disparity between $\langle P_{xy} \rangle$ increases as well.

Using a hard-sphere system, Erpenback in 1984 [91] found that at large shear rates, the particles organise themselves into 'strings' when the kinetic temperature is controlled. The presence of such string phases reduces the entropy production rate in the system. A similar behaviour is observed in the soft-shere system exemplified here. Figure 20 shows the presence of string phases in the GIK and the NH thermostatted systems for $\dot{\gamma} = 10$. These string phases occur because the thermostats employed assume the stability of the linear streaming velocity profile, even at large shear rates. When Reynolds number is high, which is what happens in cases with large shear rates, the laminar flow is unstable and eddy currents develop in the streaming velocity of the particles. The two kinetic thermostats (GIK and NH) treat these eddies as local heating and withdraw this heat from the system by suppressing the eddy formation [35]. The PB thermostat, which controls both the kinetic and the configurational temperatures, also shows string phases.

The string phases disappear when the system is thermostatted through the profile-unbiased forms of GIK and NH thermostats. These profile-unbiased forms do not assume any stable streaming velocity profile, but calculate the streaming velocity locally on the fly as it is not known *apriori*. Numerically one can achieve this by dividing the simulation box into a number of cells, and calculating their center of mass velocities [122]. Controlling only the configurational temperature, as is done in the BT thermostat, provides a unique way of resolving the issue of string phases without the *apriori* knowledge of the local streaming velocity [99,123]. As the thermostat controls the temperature based on the configurational variables, there is no necessity to separately account for the streaming velocity and the peculiar momentum. At large strain rates, the BT thermostat does not hinder eddy formation and the string phases are broken. This is evident from Figure 20 where the snapshot for the BT thermostat shows no string phase. All in all it seems to us that the configurational temperature based thermostats work the best for this class of problems.

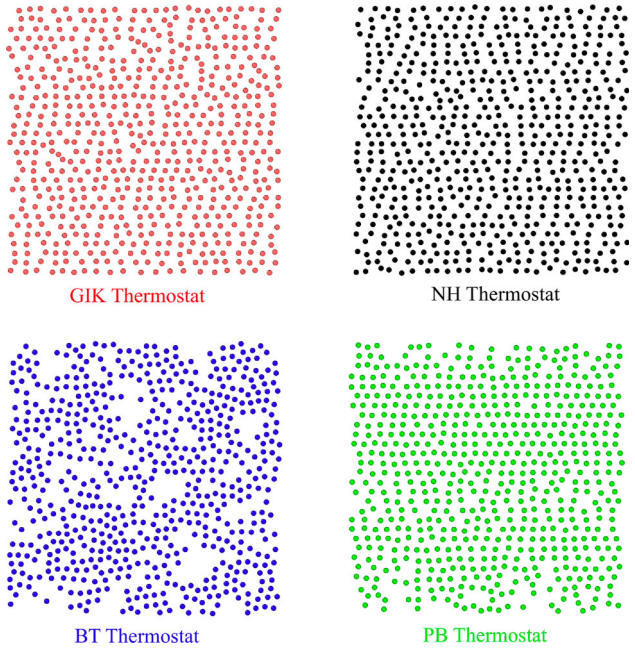

Figure 20. (Colour online) The string phases are evident in GIK, NH and PB thermostats when $\dot{\gamma} = 10$.

8. Summary & challenges ahead – open questions

In this review, we have presented different deterministic temperature control algorithms typically used in MD simulations. While most of the algorithms are offshoots of the extended system method of Nosé and Hoover, each algorithm has different advantages and disadvantages. Apart from the philosophy behind their development, we highlight – (i) the situations where they are useful, (ii) the constant of motion and Hamiltonian, if any, from which the equations of motion can be obtained, (iii) the ergodic characteristics in equilibrium using an SHO, (iv) the ability to ensure non-equilibrium thermal transport in an SHO, and (v) the transport properties in relatively larger systems. When it comes to equilibrium and small-scale systems, some of the thermostats behave similarly, for example, Nosé-Hoover, Braga-Travis, Virial, Bauer-Bulgac-Kusnezov and Patra-Bhattacharya thermostat are all non-ergodic. On the other hand, Martyna-Klein-Tuckerman, Hoover-Holian, and $C_{1,2}$ thermostats are ergodic. In fact, for an SHO, some of the thermostats have similar equations of motion.

We now discuss some of the outstanding challenges and open questions associated with thermostatted dynamics:

- Almost all deterministic thermostats discussed in this review, satisfy the extended phase-space Liouville's equation. In most of the cases, the Liouville's measure is a product of the usual canonical distribution with independent normally distributed thermostatted variables. For example, in the Nosé-Hoover thermostat, Liouville's measure is the product of the canonically distributed configurational and momentum variables with the normally distributed thermostat variable. Consider a situation where the system comprises of particles interacting harmonically with each other. For such a case, the extended phase-space distribution is the sum of independent normal variables. A philosophical issue exists with the extended phase-space distribution being the sum of independent normal distributions – the momentum evolution equation of any particle in this case is: $\dot{p}_i = -\frac{\partial \Phi}{\partial x_i} - \eta p_i$. As Φ is a harmonic function, $\partial\Phi/\partial x_i$ is linear in x. For the LHS, since p_i is a normal random variate, so is $\dot{p}_i$. However, in the RHS, while $\partial\Phi/\partial x_i$ is a normal random variate, ηp_i is a product of two normal random variables, which does not yield a normal random variate. Thus, from a statistical viewpoint, the momentum evolution equation cannot simultaneously result in momentum being normally distributed with η being normal distributed as well. This philosophical issue persists for all deterministic thermostats that rely on the extended system method. Analysis of Nosé-Hoover thermostat and its variants discussed here from this statistical viewpoint is yet

to emerge, and will possibly be able to shed more light on the ergodic characteristics of this family of thermostats.

- Moving on, one of the important question in thermostatted dynamics is related to ergodicity. While the question of ergodicity is less important in larger systems owing to prohibitively large Poincaré recurrence time, it forms the theoretical foundation for linking dynamical systems with statistical mechanics. In this regard, analytical proof of ergodicity has been given only for a limited number of cases. To the best of our knowledge, such analytical proof does not exist for any thermostatted dynamics. A particularly interesting case is that of the two-variable Martyna-Klein-Tuckerman thermostat, where for large values of Q, say $Q_\eta = Q_\xi = 10$, one observes regular trajectories which disappear for smaller values of Q such as $Q_\eta = Q_\xi = 1$. More insights into these can be obtained if the dynamics is analysed analytically.
- For larger systems, while in equilibrium the different algorithms result in similar dynamical properties since they satisfy the extended phase-space Liouville's equation, the same cannot be said in non-equilibrium. Researchers have reported non-equilibrium problems wherein thermostat-dependent properties are obtained even in near-zero nonlinearity. This begs the question – which thermostat yields correct properties. The question remains wide open for the research community to investigate, including the reason why the different thermostats show different properties. The role of a thermostat in non-equilibrium situations is to extract the extra heat from the system. So it seems that the rate at which the heat is extracted plays an important role in non-equilibrium as this rate is different for the different thermostats.
- Thermostat algorithms have been designed to control the temperature of the system to a specific value. However, researchers have reported that the temperature of a system fluctuates [124,125]. These temperature fluctuations can guide in developing better thermostat algorithms, where apart from controlling the temperature one may control the fluctuations as well. Further, a comparison of temperature fluctuations for the different thermostat algorithms in equilibrium can help in understanding which of the thermostats is, so as to speak, 'the best' for controlling temperature. Exploration in this domain seems limited owing to the contradicting views concerning the existence of temperature fluctuations in a canonical ensemble [126].
- How do the usual configurational thermostats differ from the virial thermostat? This question is at the heart of making configurational thermostats more popular. The knowledge of Hessian is must for configurational thermostats, and computing it is extremely time-consuming of the order of $\sim N^3$. Virial thermostat, on the other hand, uses the information of only forces. Thus, if the Virial thermostat performs comparably to the other configurational thermostats in different equilibrium and non-equilibrium problems, one can use Virial thermostats in lieu of the configurational thermostats. A starting point could be to compare the auto-correlation functions of velocity and energy in equilibrium and non-equilibrium scenarios. On a related note, a comparison of auto-correlation functions due to the kinetic and configurational thermostats could also shed light on the rate at which the fast (momentum) and the slow (configurational) degrees of freedom are thermostatted.
- A separate set of questions arise related to temperature measurement – (i) can one measure the configurational temperature dynamically in real-time instead of post-processing the snapshots of configurations [127,128], (ii) is it possible to uniquely measure kinetic and configurational temperatures of a system in equilibrium, and (iii) what do we measure in experiments using thermometers in away-from-equilibrium scenario. While researchers have been working towards answering these questions, satisficatory answers are yet to emerge.
- Several thermostats have a Hamiltonian associated with them – Nosé, Nosé-Hoover, Gaussian isokinetic and Virial thermostats – in the sense that the equations of motion can be derived from the usual Hamilton's equations upon suitable substitution. It is not necessary for the canonical variables to be the same as that of the real variables. The existence of Hamiltonian makes it easy to relate thermostatted dynamics with the rich physics of dynamical systems. However, several thermostats, especially the multi-variables one, do not have any Hamiltonian. An interesting line of exploration is to create suitable Hamiltonians for these thermostats.
- Gaussian isokinetic thermostat can be derived from both Gauss' principle of least constraint (the usual method) as well as the Gauss' principle of least action (through the Hamiltonian route). This suggests that the Gauss' principle of least constraint is related to Gauss' principle of least action. While the relationship between them for holonomic constraints is straight forward to show, such is not the case for non-holonomic constraints. Establishing the relationship between the two principles will pave way for an improved understanding of thermostatted dynamical systems.
- Lyapunov exponents are closely linked with time-reversibility – in an irreversible dynamical system, the sum of the Lyapunov exponents is less than zero. For a thermostatted system, apart from irreversibility, Lyapunov exponents also relate (in almost all cases) the heat-transfer entropy with the phase-space compressibility. However, such a link has only been (dis)proved for pedagogical systems. Exploration with realistic systems is yet to be observed.

Interesting progress along these and newer lines can be expected in the near future.

Acknowledgments

PKP acknowledges the support for this research provided in part by the Department of Science and Technology, Govt. of India, under the scheme DST-ECR.

Disclosure statement

No potential conflict of interest was reported by the authors.

Funding

This work was supported by Department of Science and Technology, Govt. of India [DST-ECRA, grant number ECR/2018/000340].

ORCID

Puneet Kumar Patra http://orcid.org/0000-0002-8585-8684

References

[1] Goldstein, H, Poole, Jr, CP, Safko, JL. Classical mechanics. 3rd ed. Boston (MA): Addison-Wesley; 2001.
[2] Swope, WC, Andersen, HC, Berens, PH, et al. A computer simulation method for the calculation of equilibrium constants for the formation of physical clusters of molecules: application to small water clusters. J Chem Phys. 1982;76:637.
[3] Casas-Vázquez, J, Jou, D. Temperature in non-equilibrium states: a review of open problems and current proposals. Rep Progress Phys. 2003;66:1937–2023.
[4] Haile, J. Molecular dynamics simulation. Vol. 27. New York: Wiley; 1992.
[5] Powles, JG. Negative absolute temperatures and rotating temperatures. Contemp Phys. 1963;4:338–355.
[6] Jaynes, ET. Information theory and statistical mechanics. Phys Rev. 1957;106:620–630.
[7] Jaynes, ET. Information theory and statistical mechanics. ii. Phys Rev. 1957;108:171–190.
[8] Shannon, C. A mathematical theory of communication. Bell Syst Tech J The. 1948;27:379–423.
[9] Evans, DJ. On the entropy of nonequilibrium states. J Stat Phys. 1989;57:745.
[10] Smith, W. Elements of molecular dynamics. National Center for Supercomputing Applications. 2014.
[11] Coveney, PV, Wan, S. On the calculation of equilibrium thermodynamic properties from molecular dynamics. Phys Chem Chem Phys. 2016;18:30236–30240.
[12] Sprott, JC, Hoover, WG, Hoover, CG. Heat conduction, and the lack thereof, in time-reversible dynamical systems: generalised nosé-hoover oscillators with a temperature gradient. Phys Rev E. 2014;89:042914.
[13] S., D. Ergodicity of classical billiard balls. Phys A Stat Mech Appl. 1993;194:86–92.
[14] Sinai, YG. Ergodic properties of the lorentz gas. Funct Anal Appl. 1979;13:192–202.
[15] Legoll, F, Luskin, M, Moeckel, R. Non-ergodicity of the nosé-hoover thermostatted harmonic oscillator. Arch Ration Mech Anal. 2007;184:449–463.
[16] Bulgac, A, Kusnezov, D. Canonical ensemble averages from pseudomicrocanonical dynamics. Phys Rev A. 1990;42:5045–5048.
[17] Posch, HA, Hoover, WG, Vesely, FJ. Canonical dynamics of the nosé oscillator: stability, order, and chaos. Phys Rev A. 1986;33:4253–4265.
[18] Watanabe, H, Kobayashi, H. Ergodicity of a thermostat family of the nosé-hoover type. Phys Rev E. 2007;75:040102.
[19] Zeh, H. The physical basis of the direction of time. 2001.
[20] Patra, PK, Bhattacharya, B. Nonergodicity of the nose-hoover chain thermostat in computationally achievable time. Phys Rev E. 2014;90:043304.
[21] Patra, PK, Sprott, JC, Hoover, WG, et al. Deterministic time-reversible thermostats: chaos, ergodicity, and the zeroth law of thermodynamics. Molecular Phys. 2015;113:2863–2872.
[22] Posch, HA, Hoover, WG. Time-reversible dissipative attractors in three and four phase-space dimensions. Phys Rev E. 1997;55:6803.
[23] Huang, K. Introduction to statistical physics. Boca Raton: CRC Press; 2001.
[24] Allen, MP, Tildesley, DJ, Banavar, JR. Computer simulation of liquids. Phys Today. 2008;42:105–106.
[25] Hünenberger, PH. Thermostat algorithms for molecular dynamics simulations. In Dr. Holm C and Prof. Dr. Kremer K, editors. Advanced Computer Simulation. Advances in Polymer Science. Vol. 173. Berlin Heidelberg: Springer; 2005. p. 105–149.
[26] Woodcock, LV. Isothermal molecular dynamics calculations for liquid salts. Chem Phys Lett. 1971;10:257.
[27] Martin-Löf, A. The equivalence of ensembles and the gibbs phase rule for classical lattice systems. J Stat Phys. 1979;20:557.
[28] Bussi, G, Donadio, D, Parrinello, M. Canonical sampling through velocity rescaling. J Chem Phys. 2007;126:014101.
[29] Berendsen, HJ, Postma, J v., van Gunsteren, WF, et al. Molecular dynamics with coupling to an external bath. J Chem Phys. 1984;81:3684.
[30] Braun, E, Moosavi, SM, Smit, B. Anomalous effects of velocity rescaling algorithms: the flying ice cube effect revisited. J Chem Theory Comput. 2018;14:5262–5272.
[31] Hoover, WG, Ladd, AJC, Moran, B. High-strain-rate plastic flow studied via nonequilibrium molecular dynamics. Phys Rev Lett. 1982;48:1818–1820. pRL.
[32] Evans, DJ. Computer 'experiment' for nonlinear thermodynamics of couette flow. J Chem Phys. 1983;78:3297.
[33] Evans, DJ, Morriss, GP. The isothermal/isobaric molecular dynamics ensemble. Phys Lett A. 1983;98:433–436.
[34] Evans, DJ, Morriss, GP. Isothermal-isobaric molecular dynamics. Chem Phys. 1983;77:63.
[35] Evans, DJ, Morriss, G. Statistical mechanics of nonequilibrium liquids. 2nd ed. New York: Cambridge University Press; 2008.
[36] Morriss, GP, Dettmann, CP. Thermostats: analysis and application. Chaos Interdisci J Nonlinear Sci. 1998;8:321–336.
[37] Dettmann, CP, Morriss, GP. Hamiltonian formulation of the gaussian isokinetic thermostat. Phys Rev E. 1996;54:2495.
[38] Bright, JN, Evans, DJ, Searles, DJ. New observations regarding deterministic, time-reversible thermostats and gauss's principle of least constraint. J Chem Phys. 2005;122:194106.
[39] Baranyai, A, Evans, DJ. New algorithm for constrained molecular-dynamics simulation of liquid benzene and naphthalene. Mol Phys. 1990;70:53.
[40] Evans, DJ, Morriss, GP. Shear thickening and turbulence in simple fluids. Phys Rev Lett. 1986;56:2172–2175.
[41] Morriss, GP. Lyapunov dimension of two-body planar couette flow. Phys Rev A. 1988;37:2118–2124.
[42] Evans, DJ, Sarman, S. Equivalence of thermostatted nonlinear responses. Phys Rev E. 1993;48:65.
[43] Morriss, GP, Evans, DJ. Application of transient correlation functions to shear flow far from equilibrium. Phys Rev A. 1987;35:792–797.
[44] Delhommelle, J, Evans, DJ. Configurational temperature thermostat for fluids undergoing shear flow: application to liquid chlorine. Mol Phys. 2001;99:1825.
[45] Nosé, S. Constant temperature molecular dynamics methods. Progress Theor Phys Suppl. 1991;103:1–46.
[46] Nosé, S. A unified formulation of the constant temperature molecular dynamics methods. J Chem Phys. 1984;81:511.
[47] Nosé, S. A molecular dynamics method for simulations in the canonical ensemble. Mol Phys. 1984;52:255.
[48] Andersen, HC. Molecular dynamics simulations at constant pressure and/or temperature. J Chem Phys. 1980;72:2384.
[49] Hoover, WG. Canonical dynamics: equilibrium phase-space distributions. Phys Rev A. 1985;31:1695–1697. pRA.
[50] Martyna, GJ, Klein, ML, Tuckerman, M. Nos[e-acute]–hoover chains: the canonical ensemble via continuous dynamics. J Chem Phys. 1992;97:2635.
[51] Tobias, DJ, Martyna, GJ, Klein, ML. Molecular dynamics simulations of a protein in the canonical ensemble. J Phys Chem. 1993;97:12959.
[52] Hoover, WG, Holian, BL. Kinetic moments method for the canonical ensemble distribution. Phys Lett A. 1996;211:253–257.
[53] Campisi, M, Zhan, F, Talkner, P, et al. Logarithmic oscillators: ideal hamiltonian thermostats. Phys Rev Lett. 2012;108:250601.

[54] Campisi, M, Hänggi, P. Thermostated hamiltonian dynamics with log oscillators. J Phys Chem B. 2013;117:12829–12835.
[55] Kusnezov, D, Bulgac, A, Bauer, W. Canonical ensembles from chaos. Ann Phys (N Y). 1990;204:155–185.
[56] Jellinek, J. Dynamics for nonconservative systems: ergodicity beyond the microcanonical ensemble. J Phys Chem. 1988;92:3163.
[57] Jellinek, J, Berry, RS. Generalization of nosé's isothermal molecular dynamics: necessary and sufficient conditions of dynamical simulations of statistical ensembles. Phys Rev A. 1989;40:2816–2818.
[58] Nosé, S. An extension of the canonical ensemble molecular dynamics method. Mol Phys. 1986;57:187.
[59] Hoover, WG. Computational statistical mechanics. Amsterdam: Elsevier; 1991.
[60] Dettmann, C, Morriss, G. Hamiltonian reformulation and pairing of lyapunov exponents for nosé-hoover dynamics. Phys Rev E. 1997;55:3693.
[61] Bond, SD, Leimkuhler, BJ, Laird, BB. The nosé-poincaré method for constant temperature molecular dynamics. J Comput Phys. 1999;151:114.
[62] Posch, H, Hoover, WG. Time-reversible dissipative attractors in three and four phase-space dimensions. Phys Rev E. 1997;55:6803.
[63] Searles, DJ, Evans, DJ. Fluctuation theorem for heat flow. Int J Thermophys. 2001;22:123–134.
[64] Yu, J, Zhang, S, Zhang, Q, et al. Simulation study and experiment verification of the creep mechanism of a nickel-based single crystal superalloy obtained from microstructural evolution. RSC Adv. 2016;6:107748–107758.
[65] Brańka, A, Wojciechowski, K. Generalization of nosé and nosé-hoover isothermal dynamics. Phys Rev E. 2000;62:3281.
[66] Bravetti, A, Tapias, D. Thermostat algorithm for generating target ensembles. Phys Rev E. 2016;93:022139.
[67] Sadus, RJ. Molecular simulation of fluids. Amsterdam: Elsevier; 2002.
[68] Martyna, GJ, Tuckerman, ME, Tobias, DJ, et al. Explicit reversible integrators for extended systems dynamics. Mol Phys. 1996;87:1117.
[69] Hoover, WG, Kum, O. Ergodicity, mixing, and time reversibility for atomistic nonequilibrium steady states. Phys Rev E. 1997;56:5517–5523.
[70] Liu, Y, Tuckerman, ME. Generalized gaussian moment thermostatting: A new continuous dynamical approach to the canonical ensemble. J Chem Phys. 2000;112:1685.
[71] Patra, PK, Bhattacharya, B. Zeroth law investigation on the logarithmic thermostat. Sci Rep. 2018;8:1.
[72] Hoover, WG, Hoover, CG. Hamiltonian thermostats fail to promote heat flow. Commun Nonlinear Sci Numer Simulat. 2013;18:3365–3372.
[73] Sponseller, D, Blaisten-Barojas, E. Failure of logarithmic oscillators to serve as a thermostat for small atomic clusters. Phys Rev E. 2014;89:021301.
[74] Chen, K, He, D, Zhao, H. Violation of the virial theorem and generalized equipartition theorem for logarithmic oscillators serving as a thermostat. Sci Rep. 2017;7:1.
[75] Rugh, HH. Dynamical approach to temperature. Phys Rev Lett. 1997;78:772–774.
[76] Rugh, HH. A geometric, dynamical approach to thermodynamics. J Phys A Math General. 1998;31:7761–7770.
[77] Jepps, OG, Ayton, G, Evans, DJ. Microscopic expressions for the thermodynamic temperature. Phys Rev E. 2000;62:4757.
[78] Morriss, GP, Rondoni, L. Definition of temperature in equilibrium and nonequilibrium systems. Phys Rev E. 1999;59:R5–R8.
[79] Hoover, WG, Hoover, CG. Nonequilibrium temperature and thermometry in heat-conducting ϕ 4 models. Phys Rev E. 2008;77:041104.
[80] Hoover, WG, Hoover, CG. Hamiltonian dynamics of thermostated systems: two-temperature heat-conducting ϕ 4 chains. J Chem Phys. 2007;126:164113.
[81] Baranyai, A, Evans, DJ, Daivis, PJ. Isothermal shear-induced heat flow. Phys Rev A. 1992;46:7593–7600.
[82] Ayton, G, Jepps, OG, Evans, DJ. On the validity of fourier's law in systems with spatially varying strain rates. Mol Phys. 1999;96:915.
[83] Daivis, PJ, Dalton, BA, Morishita, T. Effect of kinetic and configurational thermostats on calculations of the first normal stress coefficient in nonequilibrium molecular dynamics simulations. Phys Rev E. 2012;86:056707.
[84] Basconi, JE, Shirts, MR. Effects of temperature control algorithms on transport properties and kinetics in molecular dynamics simulations. J Chem Theory Comput. 2013;9:2887–2899.
[85] Cho, K, Joannopoulos, JD. Ergodicity and dynamical properties of constant-temperature molecular dynamics. Phys Rev A. 1992;45:7089–7097.
[86] Patra, PK, Bhattacharya, B. Heat pump without particle transport or external work on the medium achieved by differential thermostatting of the phase space. Phys Rev E. 2016;93:033308.
[87] Sri Harish, M, Patra, PK. Temperature and its control in molecular dynamics simulations, arXiv, arXiv. 2020.
[88] Butler, BD, Ayton, G, Jepps, OG, et al. Configurational temperature: verification of monte carlo simulations. J Chem Phys. 1998;109:6519.
[89] Lue, L, Evans, DJ. Configurational temperature for systems with constraints. Phys Rev E. 2000;62:4764–4768.
[90] Landau, LD, Lifshitz, EM. Course of theoretical physics, statistical physics, part 1. 3rd ed. Vol. 5. Oxford (UK): Elsevier; 1980.
[91] Erpenbeck, JJ. Shear viscosity of the hard-sphere fluid via nonequilibrium molecular dynamics. Phys Rev Lett. 1984;52:1333.
[92] Zhao, FP, An, Q, Li, B, et al. Shock response of a model structured nanofoam of cu. J Appl Phys. 2013;113:063516.
[93] He, AM, Duan, S, Shao, JL, et al. Shock melting of single crystal copper with a nanovoid: molecular dynamics simulations. J Appl Phys. 2012;112:074116.
[94] Evans, DJ, Cui, S, Hanley, H, et al. Conditions for the existence of a reentrant solid phase in a sheared atomic fluid. Phys Rev A. 1992;46:6731–6734.
[95] Travis, KP, Daivis, PJ, Evans, DJ. Thermostats for molecular fluids undergoing shear flow: application to liquid chlorine. J Chem Phys. 1995;103:10638.
[96] Braga, C, Travis, KP. A configurational temperature nos[e-acute]-hoover thermostat. J Chem Phys. 2005;123:134101.
[97] Lue, L, Jepps, OG, Delhommelle, J, et al. Configurational thermostats for molecular systems. Mol Phys. 2002;100:2387.
[98] Samoletov, AA, Dettmann, CP, Chaplain, MAJ. Thermostats for 'slow' configurational modes. J Stat Phys. 2007;128:1321.
[99] Travis, KP, Braga, C. Configurational temperature and pressure molecular dynamics: review of current methodology and applications to the shear flow of a simple fluid. Mol Phys. 2006;104:3735.
[100] Travis, KP, Braga, C. Configurational temperature control for atomic and molecular systems. J Chem Phys. 2008;128:014111.
[101] Samoletov, AA, Dettmann, CP, Chaplain, MAJ. Notes on configurational thermostat schemes. J Chem Phys. 2010;132:246101.
[102] Beckedahl, D, Obaga, EO, Uken, DA, et al. On the configurational temperature nosè–hoover thermostat. Phys A Stat Mech Appl. 2016;461:19–35.
[103] Patra, PK, Bhattacharya, B. An ergodic configurational thermostat using selective control of higher order temperatures. J Chem Phys. 2015;142:194103.
[104] Hamilton, IP. Modified nosé-hoover equation for a one-dimensional oscillator: enforcement of the virial theorem. Phys Rev A. 1990;42:7467–7470.
[105] L'Heureux, I, Hamilton, I. Canonically modified nosé-hoover equation with explicit inclusion of the virial. Phys Rev E. 1993;47:1411.
[106] Samoletov, AA, Dettmann, CP, Chaplain, MA. Thermostats for 'slow' configurational modes. J Stat Phys. 2007;128:1321.
[107] Patra, PK, Hoover, WG, Hoover, CG, et al. The equivalence of dissipation from gibbs' entropy production with phase-volume loss in ergodic heat-conducting oscillators. Int J Bifurcation Chaos. 2016;26:1650089.
[108] Watanabe, H, Kobayashi, H. Ergodicity of the nosé-hoover method. Mol Simul. 2007;33:77–81.
[109] Legoll, F, Luskin, M, Moeckel, R. Non-ergodicity of the nosé–hoover thermostatted harmonic oscillator. Arch Ration Mech Anal. 2007;184:449–463.

[110] Legoll, F, Luskin, M, Moeckel, R. Non-ergodicity of nosé–hoover dynamics. Nonlinearity. 2009;22:1673–1694.
[111] Hoover, W, Posch, H. Second-law irreversibility and phase-space dimensionality loss from time-reversible nonequilibrium steady-state lyapunov spectra. Phys Rev E. 1994;49:1913.
[112] Hoover, WG, Posch, HA. Multifractals from stochastic many-body molecular dynamics. Phys Lett A. 1998;246:247–251.
[113] Hoover, WG. Liouville's theorems, gibbs' entropy, and multifractal distributions for nonequilibrium steady states. J Chem Phys. 1998;109:4164–4170.
[114] Hoover, WG, Hoover, C, Posch, H, et al. The second law of thermodynamics and multifractal distribution functions: bin counting, pair correlations, and the kaplan–yorke conjecture. Commun Nonlinear Sci Numerical Simulat. 2007;12:214–231.
[115] Plimpton, S. Fast parallel algorithms for short-range molecular dynamics. Type Tech. Rep. Albuquerque (NM): Institution Sandia National Labs; 1993.
[116] Berendsen, HJ, van der Spoel, D, van Drunen, R. Gromacs: a message-passing parallel molecular dynamics implementation. Comput Phys Commun. 1995;91:43.
[117] Dhar, A. Heat transport in low-dimensional systems. Adv Phys. 2008;57:457.
[118] Patra, P, Bhattacharya, B. A deterministic thermostat for controlling temperature using all degrees of freedom. J Chem Phys. 2014;140:064106.
[119] Patra, PK, Batra, RC. Nonequilibrium temperature measurement in a thermal conduction process. Phys Rev E. 2017;95:013302.
[120] Lees, A, Edwards, S. The computer study of transport processes under extreme conditions. J Phys C Solid State Phys. 1972;5:1921–1928.
[121] Hoover, WG, Hoover, CG, Petravic, J. Simulation of two-and three-dimensional dense-fluid shear flows via nonequilibrium molecular dynamics: comparison of time-and-space-averaged stresses from homogeneous doll's and sllod shear algorithms with those from boundary-driven shear. Phys Rev E. 2008;78:046701.
[122] Todd, B, Daivis, PJ. Homogeneous non-equilibrium molecular dynamics simulations of viscous flow: techniques and applications. Mol Simul. 2007;33:189–229.
[123] Delhommelle, J, Petravic, J, Evans, DJ. Reexamination of string phase and shear thickening in simple fluids. Phys Rev E. 2003;68:031201.
[124] Chui, T, Swanson, D, Adriaans, M, et al. Temperature fluctuations in the canonical ensemble. Phys Rev Lett. 1992;69:3005–3008.
[125] Hickman, J, Mishin, Y. Temperature fluctuations in canonical systems: insights from molecular dynamics simulations. Phys Rev B. 2016;94:184311.
[126] Kittel, C. On the nonexistence of temperature fluctuations in small systems. Am J Phys. 1973;41:1211.
[127] Han, Y, Grier, DG. Configurational temperature of charge-stabilized colloidal monolayers. Phys Rev Lett. 2004;92:148301.
[128] Zhao, S-C, Schröter, M. Measuring the configurational temperature of a binary disc packing. Soft Matter. 2014;10:4208.